ADVANCED BIOLOGY
www.advanced-bio.com

Assessing Novel Antibody-Based Therapies in Reconstructive 3D Cell Models of the Tumor Microenvironment

*Giacomo Domenici, Nuno F. Lopes, Gonçalo Trindade, Isabella Ramella Gal, Joan Miret Minard, Sofia P. Rebelo, Catarina Freitas, Nádia Duarte, and Catarina Brito**

Targeted, combinatorial, and immunomodulatory therapies, such as antibody-drug conjugates (ADCs) and immunomodulatory antibodies (Abs), are powerful weapons against tumor cells and immune cells within the tumor microenvironment (TME). Therefore, the evaluation of such therapies should be conducted in pre-clinical models able to recapitulate the complex cellular and molecular crosstalk of the TME. To build-in critical hallmarks of the TME, a breast cancer heterotypic 3D cell model (3D-3) is devised using a microencapsulation strategy with an inert biomaterial (alginate) and agitation-based cultures. Both stromal and immune components are added to multicellular tumor spheroids, therefore fostering cancer-associated fibroblasts (CAFs) and tumor-associated macrophages (TAMs) immunomodulatory interactions. The potential of the methodology to assess Ab-based therapies is then addressed by employing a series of anti-HER2-based ADCs. ADCs induced tumor-cell specific cytotoxicity toward HER2+ breast cancer spheroids while sparing HER2-negative CAFs. In addition, an immunomodulatory blocking Ab against colony-stimulating factor 1 receptor (CSF1R) decreases the expression of immunosuppressive and anti-inflammatory markers in TAMs, like what is previously observed upon in vivo α-CSF1R administration. Collectively, the human TME-based 3D-3 cell model is a suitable tool to evaluate the anti-tumor and immunomodulatory potential of novel antibody-based therapies directed against TME targets, such as cancer cells and macrophages.

1. Introduction

Solid tumors are characterized by intricate interactions between cancer cells, stromal cells (e.g., cancer-associated fibroblasts – CAFs), and immune cells (e.g., tumor-associated macrophages – TAMs). Extracellular matrix (ECM) and soluble factors are also important players in this crosstalk and collectively, cellular and acellular components comprise the tumor microenvironment (TME).[1] It is well established that the molecular crosstalk occurring within the TME dictates tumor progression and response to therapy.[2,3]

Several advances have been made for targeted therapy toward breast cancer, with the development of inhibitors of several pathways, including BRAF, PARP, AKT, FGFR,[4–6] and monoclonal antibodies (mAbs) targeting tumor cell signaling and growth or surrounding stromal and immune cells.[7] mAbs pose as suitable candidates for targeted therapy, due to their high target specificity, low systemic toxicity, and flexibility for conjugation with diverse

G. Domenici, N. F. Lopes, G. Trindade, I. Ramella Gal, S. P. Rebelo, C. Freitas, N. Duarte, C. Brito
iBET
Instituto de Biologia Experimental e Tecnológica
Apartado 12, Oeiras 2780–901, Portugal
E-mail: anabrito@ibet.pt

The ORCID identification number(s) for the author(s) of this article can be found under https://doi.org/10.1002/adbi.202400431

DOI: 10.1002/adbi.202400431

G. Domenici, N. F. Lopes, G. Trindade, I. Ramella Gal, C. Freitas, N. Duarte, C. Brito
Instituto de Tecnologia Química e Biológica António Xavier
Universidade Nova de Lisboa
Av. da República, Oeiras 2780-157, Portugal

J. Miret Minard
Department of Chemical
Biological and Environmental Engineering
Universitat Autònoma de Barcelona
Plaça Cívica, Bellaterra 08193, Spain

molecules.[8] An example is represented by Trastuzumab (Tmab), a mAb which targets the human epidermal growth factor receptor 2 (HER2/ERBB2), overexpressed in cancer cells from 15–30% of breast cancer (BC) patients. Tmab blocks HER2-HER3 ligand-dependent dimerization, downregulating PI3K/MAPK signaling pathway.[9] Tmab also elicits an immune response by inducing Ab-dependent cell cytotoxicity (ADCC) on immune cells able to recognize the constant region (Fc) of the mAb. Other mAbs used in the clinic aim to boost the immune response by blocking immune checkpoints (ICs), impairing T-cell inhibitory signaling, and mediating antitumor adaptive responses.[10] Furthermore, mAbs that dampen the TAMs anti-inflammatory status (e.g., targeting CD47, CD40)[11,12] are also under clinical investigation. Therapeutic strategies targeting colony-stimulating factor 1 receptor (CSF1R) in TAMs are particularly interesting, as its blockade has been demonstrated to deplete TAMs from tumors or even reprogram the pro-tumorigenic phenotype.[13,14] Antibody-Drug-Conjugates (ADCs) have also shown a great impact as a therapeutic strategy against multiple malignancies, including metastatic BC[15] and many others undergoing clinical trials.[16–18] ADCs are typically composed of a mAb covalently linked to a cytotoxic substance ("payload"), combining the specificity conferred by the mAb with more effective chemotherapeutic doses.[18] ADCs developed against HER2+ BC are successful examples of this class of therapies. Tmab-DM1 (KADCYLA), in which Tmab is covalently linked to DM1 (Mertansine), a microtubule inhibitor, is now recommended as adjuvant therapy for adult patients with HER2+ BC.[19] Tmab-DM1 significantly increased 3-year disease-free survival compared to patients treated with only Tmab (88.3% versus 77%)[20] and significantly dropped the risk of recurrence by 50%.[19] More recently, Tmab-deruxtecan, (a potent topoisomerase I inhibitor), has been shown to significantly extend patient disease-free progression in 12 months.[21]

The initial assessment of the anti-tumorigenic potential of mAbs directed against TME components is usually performed in vitro, in cultures of well-established cancer cell lines and donor-derived immune cells, grown on plastic surfaces.[22] These cultures do not account for tissue tridimensionality (3D) nor the presence of a complex TME, which impacts the exposure of cancer cells to mAb and mAb diffusion.[23] The absence of 3D structure and TME interactions often results in a marked overestimation of mAb overall in vivo potency.[24] Altogether, these data highlight the need for better cell models that account for the tridimensionality of the tumor tissue, while representing the cell complexity typical of the TME. These models can improve predictive power at in vitro stages, addressing the therapeutic potential of novel Ab both in pre-clinical and co-clinical settings. Our group developed 3D co-culture cell models, by embedding multicellular cancer spheroids and relevant TME components, such as CAFs and TAMs, in alginate microcapsules. These models aim to recapitulate specific events within the TME, allowing to address relevant biological questions in controlled environments. The models rely on agitation cultures to improve nutrients and gas diffusion,[25] which greatly increases the lifespan of the reconstructed 3D TME, as we have previously shown.[26] The cellular complexity of this versatile model can be sequentially increased, as cancer spheroids can be cultured alone[27] or with human fibroblasts, which increase collagen deposition and build a pro-inflammatory environment.[28] In addition, we developed a 3D-3 cell culture system, where cancer spheroids are co-cultured with both fibroblasts and monocytes,[29] the latter differentiating into TAMs and recapitulating an anti-inflammatory cytokine secretory *milieu*. Previous data showed that 3D-3 models are amenable to test TAM immunomodulators like the CSF1R chemical inhibitor BLZ945, which showed a reduction in the proportion of TAMs ($CD163^+/CD206^+$) within the myeloid compartment.[29] Other studies by our group have shown the potential for Ab diffusion within alginate microcapsules and the impact of Tmab and Pertuzumab on the phenotype of peripheral blood mononuclear cells (PBMCs), co-cultured with HER2+ cell lines.[30] Together, these observations suggest that our co-culture methodology can be used to assess the therapeutic potential of mAbs.

In this study, we aimed to assess the amenability of our TME models to test the potency and specificity of ADCs and immunomodulatory mAbs. For this, we employed two 3D co-culture cell models, to address specific biological questions for each therapeutic modality. First, we microencapsulated multicellular spheroids from HER2+ BC cell lines in mono- or co-culture with human fibroblasts (hFs). The co-cultures were exposed to Tmab-based ADCs, to characterize the impact of different payloads and conjugation strategies. For the immunomodulatory Abs, we took a two-step approach. Co-cultures of multicellular spheroids from different BC cell lines and human monocytes were established, to explore cues underlying TAM modulation in a more controlled environment. Afterward, the complexity of the model was increased by establishing 3D-3 cultures composed of triple-negative BC (TNBC) spheroids, hFs, and monocytes. We challenged such cultures with a CSF1R blocking antibody (α-CSF1R)[31] and observed its impact on TAM phenotype. Collectively, this work shows that our methodology for 3D co-culture cell models can be used to evaluate the potential of novel mAb-based therapies, with different mechanisms of action.

2. Results

2.1. Exploring 3D Cell Models of HER2+ BC Microenvironment to Assess Anti-HER2 ADC Activity

To assess the impact of Tmab-derived ADCs on BC cells, we implemented two different HER2+ BC models, employing a 3D co-culture strategy previously reported by our team.[28,30] We generated multicellular cancer spheroids of two HER2+ BC cell lines: BT474 and HCC1954,[32] while BT474 are reported to be sensitive to Tmab, HCC1954 contain a mutation in PIK3CA that confers resistance to the mAb.[33] The BC spheroids were microencapsulated in alginate alongside hFs and co-cultured for two weeks (**Figure 1A**). To assess the impact of stromal cells on ADCs effect, 3D monocultures of BC spheroids were used as control. After 2 weeks of culture, high viability was observed for cancer cells and hF in mono and co-cultures of both BC cell lines, with few dead cells (Figure 1B; Figure S1A,B, Supporting Information). A positive control of cell death is shown in Figure S1C (Supporting Information). The hFs were well distributed throughout the alginate microcapsules (Figure 1B). We could also observe an increase in HCC1954 spheroid diameter from 1 to 2 weeks in mono- and co-cultures (Figure 1C), similar to what was observed previously in MCF-7 BC spheroids/hFs co-cultures.[28] Nevertheless, no differences were detected in

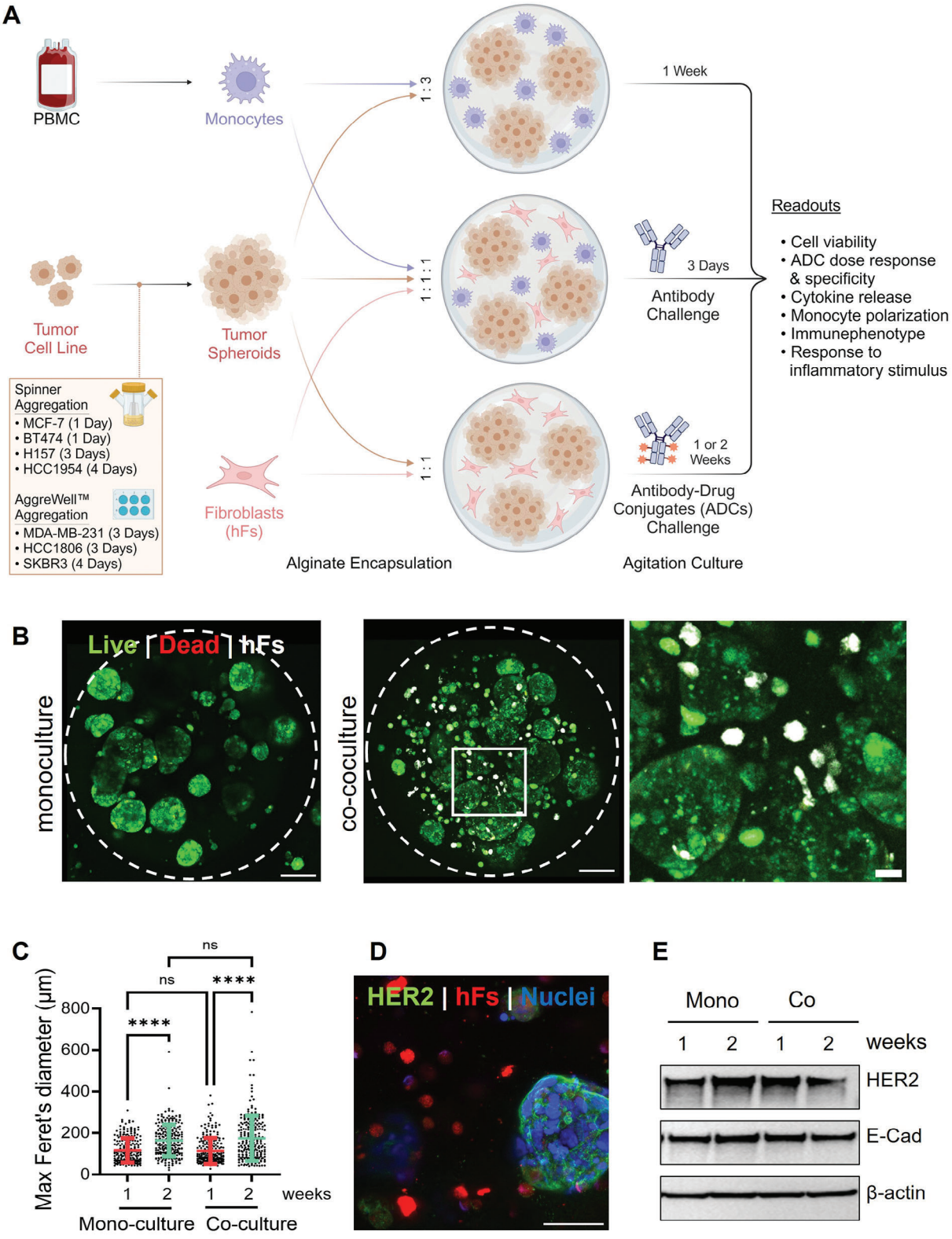

Figure 1. 3D cell co-cultures of tumor cell spheroids and hFs. A) Increasing cell complexity can be achieved in alginate microcapsules by co-culturing cancer cell line-derived spheroids with fibroblasts, blood-derived monocytes or both in alginate capsules cultured under agitation. Challenges with Antibody-drug Conjugates (ADCs) and immunomodulatory antibodies can be performed. B) Assessment of cell viability by Calcein-AM, live cells; TO-Pro®-3, dead cells in 2-weeks monocultures of HCC1954 BC spheroids mono- and co-cultures with human dermal fibroblasts (hFs), stained with CellTrace yellow. Scale bar: 100 µm in B and C and 20 µm in D. Images obtained by confocal microscopy (Mica, Leica) and showed as max projection of 38 slices

(monocultures) and 91 slices (co-cultures) of 1 µm. C) HCC1954 BC spheroid size distribution in mono- and co-culture with hDF after 1 and 2 weeks of encapsulated culture. Data are shown as mean ± SD of 232 spheroids from 3 independent experiments. Statistical analysis was performed with the non-parametric Kruskal Wallis test with Dunn's correction (**** $p < 0.0001$). D) Immunofluorescence detection for HER2 and confocal microscopy of a 2-weeks encapsulated co-culture of HCC1954 spheroid (HER2, green) with hFs stained with CellTrace Yellow prior to encapsulation (red). Nuclei were counterstained with DAPI (blue); Scale bar: 50 µm. E) Western blot showing HER2 and E-cadherin (E-cad) in encapsulated HCC1954 mono- and co-cultures (Co) with hFs. β-actin was used as loading control. Abbreviations: Mo: monoculture; Co: co-culture; hFs: fibroblasts; ns: not significant.

HCC1954 spheroid diameter cultured alone or with hFs, at 1 and 2 weeks (Figure 1C). HCC1954 cells further showed to maintain the surface expression of HER2 along culture (Figure 1D,E; Figure S1D, Supporting Information), whereas no detection of the receptor was observed in hFs, cultured either in 2D monolayers (Figure S1E,F, Supporting Information) or 3D co-cultures (Figure 1D). In addition, the expression of E-cadherin, involved in cell-to-cell adhesion, was also maintained along HCC1954 cultures, indicating the formation of compact cancer spheroids, even in the absence of hFs (Figure 1E). Similar results were observed for BT474 (Figure S1G,H, Supporting Information). These results indicated the amenability of the 3D heterotypic co-culture models for the evaluation of Tmab-ADC cytotoxic and specific effects against HER2+ cells.

2.2. Assessing the Cytotoxic Potential of Different Anti-HER2 ADCs on 3D Heterotypic Co-cultures

To assess the cytotoxic effects of ADCs against HER2+ BC microencapsulated spheroids, we synthesized a series of Tmab-derived ADCs with different cytotoxic payloads (MMAE and DM1, previously used in[34,35]), employing different chemical synthesis strategies (heterogeneous/homogenous conjugation).[36] The newly synthesized ADCs (**Table 1**) comprised different payload numbers, conjugated to the mAbs through different linkers. Control mAbs were also synthesized, including Tmab and Tmab_cys114, the latter with a site-specific amino acid modification to facilitate MMAE homogeneous conjugation. All mAbs were extensively characterized (described in Supporting Materials and Methods, Supporting Information); SDS-PAGE under reducing and non-reducing conditions (Figure S2A, Supporting Information) showed the typical ADC electrophoretic pattern.[37]

Following these findings, we next assessed the cytotoxic effects of those ADCs in our 3D cell cultures. We first determined ADCs cytotoxicity on 2D cultures of HCC1954 cells. ADCs significantly reduced cell viability in a dose-dependent manner while Tmab and Tmab_cys114 did not affect cell viability (Figure S2B,C, Supporting Information). We next assessed the effect of ADCs against 3D HER2+ BC cultures. BT474 and HCC1954 monocultures were challenged for up to 2 weeks with a 5 fold serial dilution (starting from 10 µg mL^{-1}) of Tmab_cys114-MMAE2 and cell death was analyzed by LDH assay.[38] Both BT474 and HCC1954 cultures showed time- and dose-dependent cell death after exposure to Tmab_cys114-MMAE2 (**Figure 2A,B**), with the highest cell death observed after 2 weeks of exposure (BT474 = EC_{50}: 0.06 µg mL^{-1}; HCC1954 = EC_{50}: 0.057 µg mL^{-1}). We then assessed the effects of other ADCs, both in HCC1954 3D microencapsulated monocultures and co-cultures with hFs. All ADC species induced cytotoxicity, when compared to Tmab, even in the presence of hFs (Figure 2C; Figure S2D,E Supporting Information). Interestingly, the LDH assay showed that ADC-induced cell death was significantly reduced in co-cultures compared to monocultures, for Tmab-MMAE4 and Tmab-MMAE8

Table 1. Monoclonal antibodies, cytotoxic conjugated drugs, and Antibody-drug conjugates (ADCs) employed in this study. Abbreviation: Tmab: Trastuzumab; Trastuzumab_cys114 (thiomab – genetically modified trastuzumab with added cysteine at position 114); DM1: Emtansine (maytansinoid-derived microtubule inhibitor); MMAE: Monomethyl auristatin E (auristatin-derived microtubule inhibitor); Tmab-DM1: Trastuzumab emtansine; Tmab-MMAE4: Trastuzumab monomethyl auristatin E; Tmab-MMAE8: Trastuzumab monomethyl auristatin E; Tmab_cys114-MMAE2: Trastuzumab_cys114 monomethyl auristatin E; DAR: Drug Antibody Ratio; SMCC: Succinimidyl 4-(N-maleimidomethyl)cyclohexane-1-carboxylate; VC: valine-citrulline; PAB: p-aminobenzylcarbamate.

Therapeutic modality	Therapeutic	MW [kDa]	Linker	Conjugation	DAR
mAb	Tmab	145.6	–	–	–
mAb	Tmab-cys114	145.6	–	–	–
Drug	DM1	0.7	–	–	–
Drug	MMAE	0.7	–	–	–
ADC	Tmab-DM1	148.4	SMCC (non-cleavable thioether)	Heterogeneous (site-directed conjugation–native lysines)	3
ADC	Tmab-MMAE4	150.1	vc (protease-cleavable valine-citrulline) + PAB spacer	Heterogeneous (site-directed conjugation–native cysteines-partial reduction)	4
ADC	Tmab-MMAE8	155.2	vc (protease-cleavable valine-citrulline) + PAB spacer	Homogeneous (site-directed conjugation–native cysteines-full reduction)	8
ADC	Tmab_cys114-MMAE2	148.0	vc (protease-cleavable valine-citrulline) + PAB spacer	Homogeneous (site-directed conjugation–added cysteines-thiomab)	2

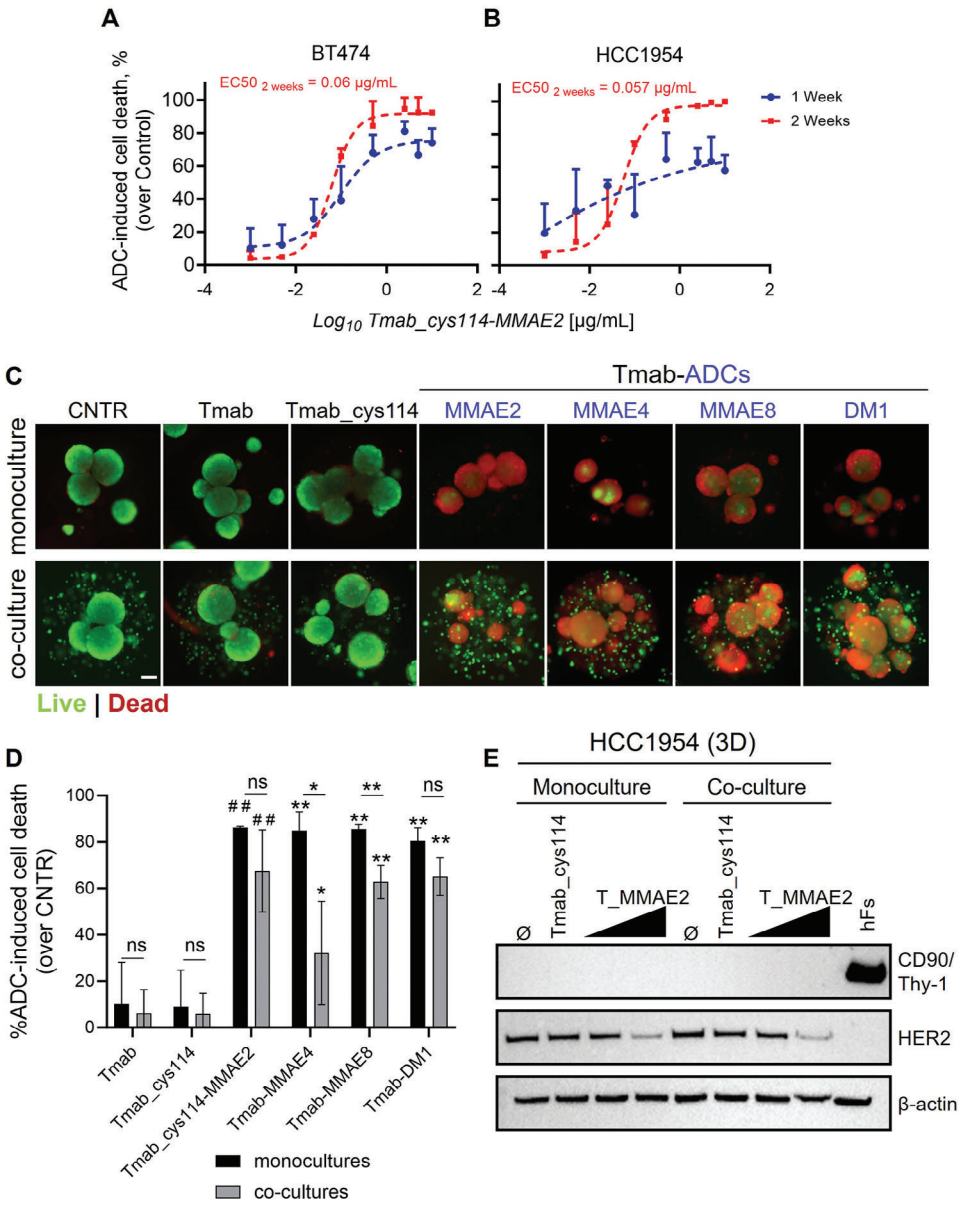

Figure 2. Trastuzumab-derived ADCs-induced cytotoxicity in HER2+ BC cell line spheroids in encapsulated 3D cultures. Effect of Tmab-cys114-MMAE2 cytotoxicity against A) BT474 and B) HCC1954 encapsulated spheroids assessed by LDH assay. Values are represented as percentage (%) of ADC-induced cell death relative to vehicle control. Data shown as mean ± SD of n = 2 independent experiments performed in triplicate. Dashed lines represent nonlinear 4 parameter (4PL) regression of Log_{10} Tmab_cys114-MMAE2 [µg mL^{-1}]. C) Representative FDA (live cells, green) and TO-Pro®-3 (dead cells, red) staining of encapsulated HCC1954 BC spheroid mono- and co-cultures with hFs encapsulated spheroids cultures exposed to different ADCs. Scale bar: 100 µm. D) ADC-induced cell death upon 2-weeks exposure to different ADCs molecules (33 nM) against HCC1954 spheroids in mono and co-cultures with hFs, assessed by LDH assay. Data shown as mean ± SD of n = 3 performed in triplicate and shown as percentage (%) of ADC-induced cell death over unchallenged condition (CNTR). Statistical analysis was performed by t-test with Welch correction, comparing each condition both with Control (CNTR, vehicle-challenged cultures) and between specific ADC exposure in mono and co-cultures. ##: $p < 0.01$ compared to Tamb_cys114; *: $p<0.05$, **$p<0.01$. E) Western blot showing protein detection levels of CD90/Thy-1 and HER2 in the HCC1954 3D fraction retrieved as shown in A from monocultures and co-cultures with hFs after exposure to 3.3 and 33 nM of Tmab with modified alanine to cysteine residue conjugated to 2 MMAE molecules (T_MMAE2, Tmab_cys114-MMAE2), and 33 nM of Tmab with modified alanine to cysteine residue (Tmab_cys114) used as ADC control. β-actin was used as loading control. Abbreviations: hFs: Human Dermal Fibroblasts; Tmab: trastuzumab; Tmab_cys114: Trastuzumab with modified alanine to cysteine residue; Tmab_cys114-MMAE2: Trastuzumab with modified alanine to cysteine residue, conjugated to 2 MMAE molecules (Maitansine, cytotoxic drug) molecules; Tmab-MMAE/4/8, trastuzumab conjugated to 4 or 8 MMAE molecules; Tmab-DM1: Trastuzumab conjugated to DM1 (Mertansine, cytotoxic drug), ns: not significant.

(Figure 2D). Tmab-ADCs were specifically cytotoxic against cancer cell spheroids, which was also confirmed by apoptotic cell detection by Nucview AF88 staining (Figure S2E, Supporting Information). The inability of the Tmab-ADCs to induce hFs cytotoxicity is consistent with the lack of HER2 expression in these cells (Figure S1D,E,F, Supporting Information).

ADC challenge in scaffold-free cultures, generated in ultra-low attachment plate (ULA), induced a complete disaggregation of the original 3D cell structure (Figure S2F, Supporting Information). In contrast, the 3D structure was maintained in spheroids upon microcapsule chelation, which enabled us to quantify the mean intensity of FDA (live cells) and TO-Pro-3 (dead cells) in individual spheroids, both from HCC1954 monocultures and HCC1954/hFs co-cultures (Figure S2G, Supporting Information) after ADC challenge. Monocultures and co-cultures exposed to Tmab_cys114-MMAE2 presented a striking decrease in the FDA/TO-Pro-3 mean intensity ratio per spheroid compared to control cultures or cultures challenged with non-ADC control mAb.

The maintenance of the spheroid 3D structure upon microcapsule chelation paved the way for the setting up of a straightforward protocol for spheroid separation from the surrounding stromal cells. With this aim, we coupled alginate chelation with filtration through cell a 40 µm strainer (Experimental Section and Figure S1, Supporting Information). To assess contamination with hFs in isolated cancer cell spheroids, we used the mesenchymal marker CD90/Thy-1, highly expressed by hFs.[39] Accordingly, CD90 was detected in hFs but was absent in HCC1954 cell fraction, cultured both in 2D monolayers and 3D cultures (Figure S2H, Supporting Information). Western blot analysis of HCC1954 3D monocultures and co-cultures with hFs confirmed the absence of CD90 in the isolated cancer cell fractions. Interestingly, cultures challenged with Tmab_cys114-MMAE2 showed a reduction in HER2 expression (Figure 2E), in agreement with a previous study with another HER2-targeting ADC, Tmab-DM1, both in lung adenocarcinoma[40] and HER2+ BC cell lines.[41] Altogether, these data showed that the 3D cell culture methodology herein presented is a suitable platform to analyze ADC cytotoxic and cell-specific effects, both in monotypic and heterotypic 3D cancer cell cultures.

2.3. Assessing Macrophage Phenotype in 3D BC Heterotypic Co-cultures

Aiming to address immunomodulatory Ab-based therapies, heterotypic co-cultures were implemented by microencapsulating multicellular BC spheroids with naïve human monocytes (Figure 1A). Six BC cell lines were used, surrogates for the luminal (MCF-7, BT474), HER2-overexpressing (SKBR-3, HCC1954), and triple negative (HCC1806, MDA-MB-231) BC subtypes.[42] Prior to microencapsulation, monocytes were labeled with CellTracker Deep Red, to ease monitorization along the culture. One week post-culture setup, all co-cultures presented the retention of a myeloid fraction, as shown by the detection of CD45, a pan leukocyte marker,[43] by flow cytometry. HCC1954, HCC1806, and MDA-MB-231 showed a significantly higher fraction of myeloid cells (10.6 ± 2.9%, 6.0 ± 1.9%, and 15.2 ± 13.5% of CD45+ cells, respectively) over BT474 (1.8 ± 1.8% of CD45+ cells) (**Figure 3**A). MDA-MB-231 and HCC1954 also showed a significantly higher myeloid fraction over SKBR-3 co-cultures, (2.3 ± 0.2% of CD45+ cells). The differences in the proportion of the myeloid population between co-cultures did not seem to be correlated with the proliferative ability of the tumor cell lines in heterotypic co-cultures (Figure S3A, supporting information). The co-cultures with higher myeloid fractions, MDA-MB-231, HCC1954, and HCC1806, were chosen to pursue phenotypic characterization, along with BT474 as a control cell line. CD45+ cells showed an immunosuppressive population, with over 50% of the myeloid cells expressing both CD206 and CD163, in the four co-cultures (Figure 3B; Figure S3B, Supporting Information). Given their immunosuppressive phenotype, we labeled these myeloid cells as TAMs.[44] Of note, TAMs from HCC1954, HCC1806, and MDA-MB-231 co-cultures showed a significant increase of at least 2.5 fold in the median fluorescence intensity (MFI) of CD206 over BT474 (Figure 3C). Interestingly, TAMs from MDA-MB-231 co-cultures further showed a significant increase in CD206 over HCC1806. CD80, an inflammation-related marker,[45] was also assessed in the myeloid population, showing low intensity (Experimental Section and Figure S2, Supporting Information). No differences in CD163 and CD80 MFI were observed among co-cultures (Figure 3C).

The TAM phenotype observed in BC co-cultures suggested the establishment of an immunosuppressive microenvironment, enriched in soluble factors mediating tumor progression. To uncover these cues, the secretory profile of the co-cultures was characterized. M-CSF, a prime cytokine for monocyte recruitment and macrophage survival,[46] was quantified alongside lactate, known to mediate TAM maturation toward an immunosuppressive phenotype.[47] M-CSF was only detected in MDA-MB-231 co-cultures, with an average concentration of 27.5 ± 2.8 ng mL^{-1} (Figure 3D). Lactate concentration was higher in the culture medium of HCC1954 and MDA-MB-231 co-cultures than in those of HCC1806 and BT474 (Figure 3E).

To complement the analysis, the conditioned medium from BT474, HCC1954, HCC1806, and MDA-MB-231 co-cultures was also screened by cytokine array (Figure S4, Supporting Information). All co-cultures showed a tendency for higher detection in C-C motif chemokine ligand (CCL) 2 and C-X-C motif chemokine ligand (CXCL) 8 (CXCL8/IL-8) and CXCL5, over BT474. These chemokines were described to mediate the recruitment of monocytes within the tumor mass and mediate different stages of tumor progression and metastasis.[48,49] Analysis of HCC1954 and HCC1806 culture medium further suggested higher detection of extracellular matrix remodeling factors tissue inhibitor of metalloproteinase (TIMP) 1 and 2 and Osteopontin.[40] CXCL1, Flt-3, and PIGF were detected in higher amounts in HCC1806 and MDA-MB-231 co-cultures, reported to induce cell migration, via TAM activation.[50,51]

2.4. Assessing Immunomodulatory Agents on the 3D-3 Cultures

To seize the effect of immunomodulatory agents within the complex cellular landscape of the TME, we took advantage of the modularity of our 3D system and added both the stromal and immune components (Figure 1A). This 3D-3 culture system recapitulates cell-cell interactions between the tumor cells, the

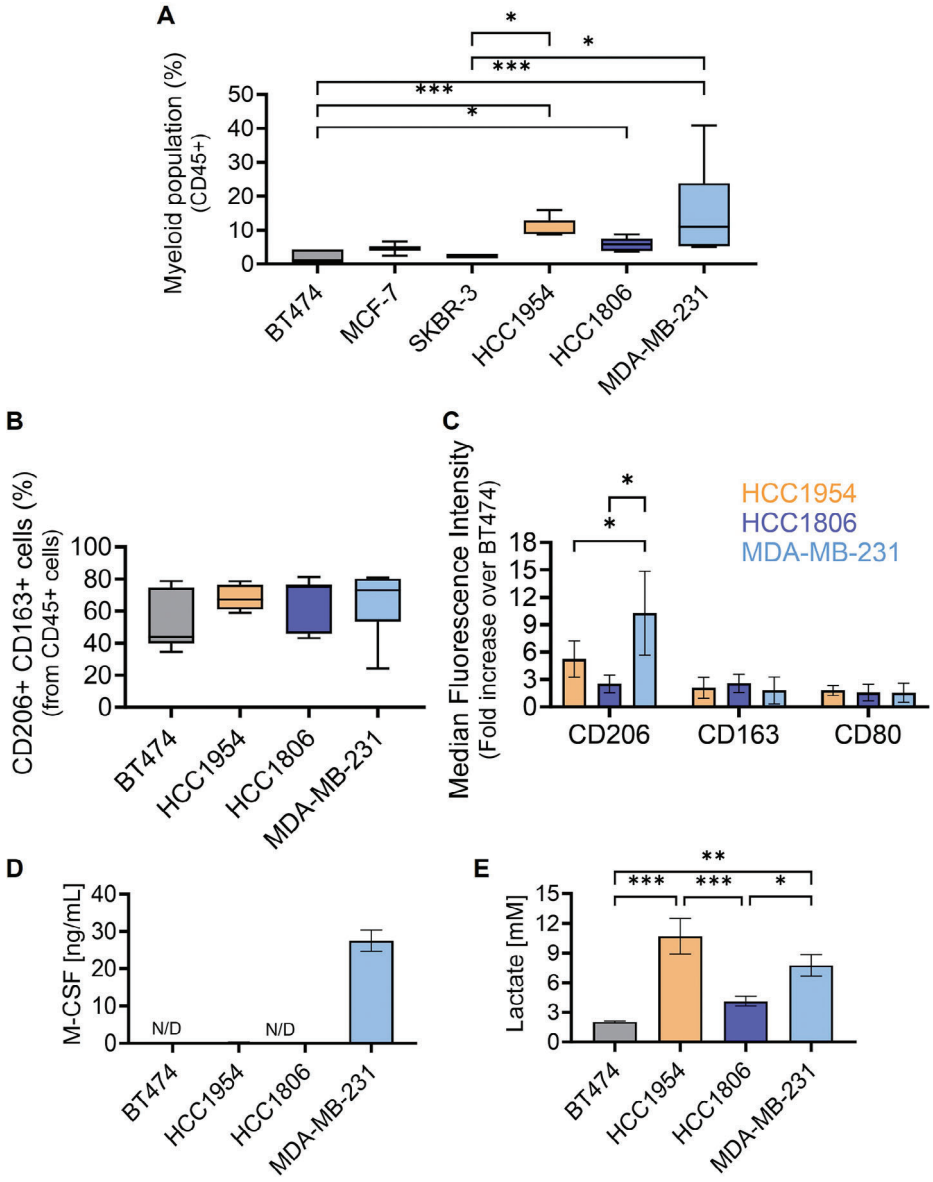

Figure 3. Characterization of BC cell spheroids/macrophage co-cultures. A) Quantification of the myeloid fraction (CD45+) among BC 3D co-cultures, by flow cytometry. Data are shown as mean of CD45+ population ± SD (n = 3 for MCF-7 and SKBR-3 & n = 6 for BT474, HCC1954, HCC1806 and MDA-MB-231 cell lines). Statistic: One-way ANOVA analysis (*: $p<0.05$; ***: $p<0.001$). B) Analysis of immunosuppressive macrophages populations in BC co-cultures, by flow cytometry. Data are shown as mean of percentage (%) of positive cells for Alexa Fluor 488 (CD206) and Alexa Fluor 647 (CD163 and CD80) ± SD (n = 6). Statistic: Two-way ANOVA analysis, followed by Tukey's multiple comparison test (*: $p<0.05$). C) Analysis of immune markers at the surface of CD45+ macrophages in BC co-cultures, by flow cytometry. Data are shown as mean of median fluorescence intensity for Alexa Fluor 488 (CD206) and Alexa Fluor 647 (CD163 and CD80) ± SD (n = 6). Statistic: One-way ANOVA analysis, by Tukey's multiple comparison test (*: $p<0.05$). D) M-CSF secretion analysis by ELISA. Data are presented as mean concentration, in ng mL^{-1} ± SD (n = 3); N/D: Not Detected. E) Lactate secretion analysis, performed via Cedex® Bio Analyzer. Data are presented as mean concentration of Lactate, in mM ± SD (n = 3). Statistic: One-way ANOVA analysis (*: $p<0.05$, **: $p<0.005$, ***: $p<0.001$).

fibroblasts, and the myeloid counterparts critical in regulating tumor progression.[29] For that, we co-cultured multicellular spheroids from the TNBC cell lines, MDA-MB-231 and HCC1806, with hFs and monocytes (3D-3 cultures, Figure 1A and **Figure 4**). We aimed to reconstruct the TME of TNBC subtypes enriched in TAMs, which modulate various oncogenic processes including cell proliferation, metastasis, and immunosuppression.[52–54] Different assays were then implemented to validate the amenability of the TME 3D cell model to evaluate the therapeutic efficacy of immunomodulatory mAbs, employing an anti-CSF1R as a proof-of-concept.[55]

After 1 week of culture, 3D-3 cultures showed high cell viability, with few dead cells (Figure 4A, left; Figure S5A, Supporting Information). All cell components appeared well distributed within alginate microcapsules, which was further confirmed by the detection of EGFR and CD45 at the surface of

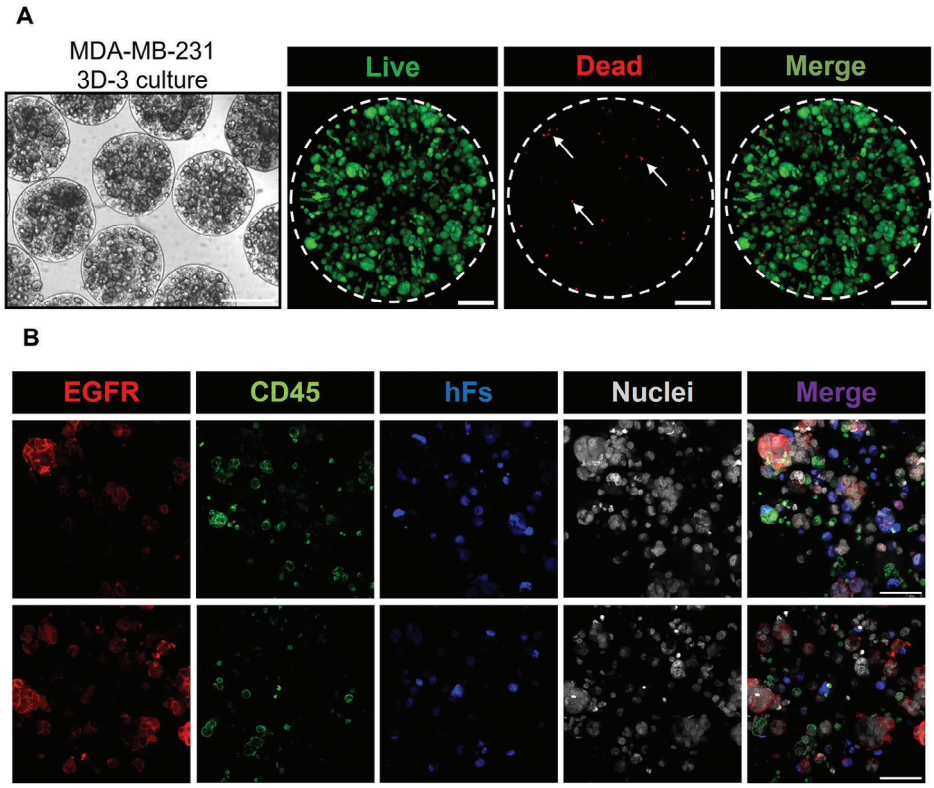

Figure 4. MDA-MB-231 3D-3 culture cell viability and immunofluorescence analysis. A) Phase-contrast image showing encapsulated 3D-3 co-cultures composed by MDA-MB-231 3D spheroids, hFs and macrophages. Scale bar: 500 µm. Calcein-AM: live cells; PI (Prodium Iodide): dead cells. Scale bar: 100 µm. B) Confocal immunofluorescence of MDA-MB-231 3D-3 cultures (EGFR-red; CD45-green; hFs-blue). Nuclei were counterstained with DRAQ5 (gray). Scale bar: 50 µm.

MDA-MB-231 and macrophages, respectively, and CellTrace dye in hFs (Figure 4B).

To assess whether these TNBC 3D-3 cultures respond to immunomodulatory stimuli, we challenged the co-cultures with TNF-α, a well-known inflammatory stimulus.[56] We observed increased secretion of the chemokines RANTES/CCL5 and IL-8/CXCL8 compared to controls (Figure S5B,C, Supporting Information), known to be induced by TNF-α.[57,58] These results suggest that the system can respond to pro-inflammatory agents. We next sought to assess the phenotypical modulation of the myeloid compartment in TNBC 3D-3 cultures exposed to anti-CSF1R molecules. We have previously shown that inhibition of CSF1R signaling with BLZ945 reduces the TAM-like anti-inflammatory phenotype ($CD163^+/CD206^+$) of myeloid cells in H157 3D-3 cultures.[29] Here, we challenged 3D-3 cultures with BLZ945 and observed a decrease in the proportion of $CD45^+/CD163^+/CD206^+$ myeloid cells (Figure S5D, Supporting Information). In addition, we tested if a commercially available anti-CSF1R blocking Ab (α-CSF1R)[31] would cause a similar effect on myeloid cells in our 3D-3 cell models. With this aim, we employed the MDA-MB-231 TNBC cell line to establish 3D-3 cultures, since these cells actively secrete M-CSF,[59] as we also confirmed (Figure 3D), which sets optimal conditions for the α-CSF1R mAb to block M-CSF extracellular binding to CSF1R. The binding of α-CSF1R mAb to CSF1R expressed at the surface of macrophages was confirmed by flow cytometry analysis (Figure S5E, Supporting Information). Furthermore, pre-incubation of macrophages with the α-CSF1R mAb markedly reduced the ability of a fluorescent-labelled anti-CSF1R mAb to detect CSF1R, confirming that the blocking mAb efficaciously recognizes its target (Figure S5F, Supporting Information). Exposure of macrophages to a range of α-CSF1R mAb concentrations did not affect their metabolic activity and cell viability (Figure S5G,H, Supporting Information), ruling out potential detrimental effects of the antibody on macrophages. Next, we assessed the effect of the α-CSF1R mAb in MDA-MB-231 3D-3 cultures, using the chemical CSF1R inhibitor BLZ945 in parallel as positive control. We observed that the expression of anti-inflammatory genes such as *MRC1*, *CD163*, *DC-SIGN* and *CSF1R*[60,61] were downregulated by CSF1R inhibition either upon challenge with BLZ945 or α-CSF1R mAb (**Figure 5A**). Furthermore, flow cytometry analysis indicated that the percentage of anti-inflammatory TAM populations ($DC\text{-}SIGN^+/CSF1R^+$) within the myeloid population of the 3D-3 co-cultures showed a tendency for a reduction upon exposure to BLZ945, which became significant with the α-CSF1R mAb (Figure 5B,C). Conversely, the population of $DC\text{-}SIGN^-/CSF1R^-$ macrophages increased upon α-CSF1R challenge (Figure 5D). We observed that such divergent populations were characterized by different levels of other TAM markers, namely CD206 and CD163, which were more expressed in $DC\text{-}SIGN^+/CSF1R^+$ than in $DC\text{-}SIGN^-/CSF1R^-$ macrophages (Figure 5B; Figure S5I, Supporting Information). This suggests a co-expression pattern for CD206, CD163, CSF1R, and DC-SIGN and highlights the

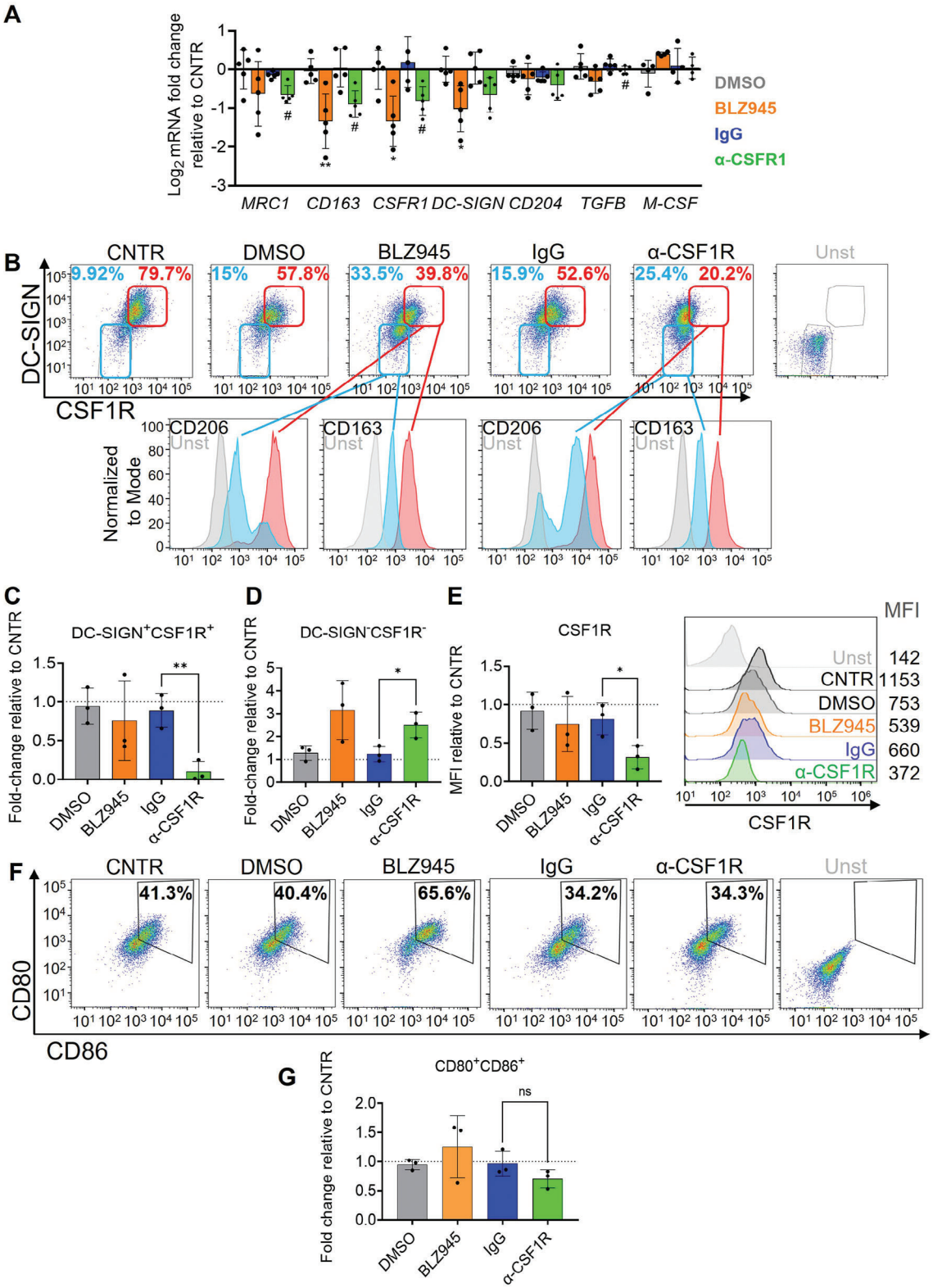

Figure 5. Immunomodulatory effect of BLZ945 and anti-CSF1R antibody in 3D-3 MDA-MB-231 encapsulated cultures. A) Gene expression analysis by RT-qPCR of a set of anti-inflammatory genes in 3D-3 co-cultures upon challenge with DMSO, BLZ945, IgG and anti-CSF1R (α-CSF1R). Data are shown as mean Log2 Fold change ±SD mRNA expression (n = 5) compared to unchallenged control condition. Statistic: Mann-Whitney nonparametric test, comparing DMSO versus BLZ945 (*: $p<0.05$, **: $p<0.01$) and IgG versus anti-CSF1R (#: $p<0.05$). CNTR, non-challenged cultures. B) Representative flow cytometry DC-SIGN/CSF1R dot-plot detection in CD45^{+}/7AAD^{-} macrophages (live cells) retrieved from MDA-MB-231 3D-3 cultures after exposure to DMSO, BLZ945, IgG and anti-CSF1R (α-CSF1R). Percentage of cells in each coloured box is shown (DCSIGN^{+}/CSF1R^{+}: red, DC-SIGN^{-}/CSF1R^{-}: blue).

presence of a heterogeneous myeloid population within 3D-3 cultures. *In-silico* analysis of gene expression performed in the R2 Genomics Analysis and Visualization Platform–AMC, showed that both CD206 (*MRC1*) and *CD163* positively correlate with the expression of either *CSF1R* or DC-*SIGN* (R-value > 0; GSE142102,[62] n = 226; and GSE76124,[63] n = 198), corroborating our observations (Tables S1 and S2, Supporting Information). Furthermore, we observed that CSF1R detection in macrophages was strongly reduced upon challenging 3D-3 cultures with the α-CSF1R mAb, compared to control IgG (Figure 5E). Our data showed a time-dependent reduction in α-CSF1R detection at the macrophage cell surface, indicating significant internalization of the α-CSF1R early upon mAb exposure (Figure S5J, Supporting Information). These data indicate that CSF1R inhibition dampened the expression of anti-inflammatory-like markers in TAMs from MDA-MB-231 3D-3 cultures, though it did not increase the expression of pro-inflammatory-like markers. Typical pro-inflammatory myeloid markers were not significantly modulated by CSFR1 inhibition, both at gene (Figure S5K, Supporting Information) and protein level (CD80 and CD86, Figure 5F,G). Finally, we observed that inhibition of CSF1R, both with BLZ945 and α-CSF1R mAb, did not affect macrophage viability in 3D-3 cultures (Figure S5L, Supporting Information), similar to what was observed in 2D cultures (Figure S5G,H, Supporting Information). In conclusion, CSF1R immunomodulation dampened TAM phenotype within 3D-3 microencapsulated co-cultures without a detrimental effect on their viability.

3. Discussion

Here, we implemented 3D BC cell models with adjustable cellular complexity, based on the entrapment of different cell types of the TME within an inert scaffold and agitation-based cultures. This modular platform was shown to be amenable for the assessment of ADCs potency, specificity, and mode of action, and for the analysis of the immunomodulatory potential of novel mAbs.

By using HER2-targeting ADCs (Tmab-ADCs) we observed tumor cell-specific killing in alginate-microencapsulated 3D co-cultures of HER2+ tumor cells and hFs. Under the experimental conditions applied, hFs do not affect HER2 expression in HCC1954 spheroids nor spheroid diameter. Since patients resistant to Tmab are the primary candidates for Tmab-ADCs, HCC1954 was specifically chosen as a cell model,[33] as it allows to study of the effect exerted by the conjugation of the payload relative to the mAb alone. We did not observe hFs cytotoxicity upon ADC challenge, potentially as the result of the lack of HER2 expression on hFs and their negligible cell proliferation within alginate microcapsules.[28] The latter would make them resistant to the by-stander cytotoxic ADC payloads MMAE and DM1 released by dying cancer cells. To our knowledge, this is the first report of the application of a heterotypic 3D cell model to assess ADC activity and specificity. Perspective application of 3D cell models will include the analysis of the potential of ADCs directed against stromal components,[35] evaluating their bystander effect on cancer cells.[64,65] Given the potential of this 3D co-culture methodology to incorporate both cancer cells and CAFs, we are convinced that our cell models provide an excellent in vitro tool to assess preclinically DAaRTS (drug activation and release through stroma) related events. The transparency of alginate microcapsules[66] will further ensure the visualization of DAaRTS-related cytotoxic effects toward cancer cells, upon stromal-ADC exposure.

In addition, this heterotypic 3D cell culture methodology will be a very helpful tool to analyze targeted therapy resistance mechanisms and to unravel specific cell-cell interaction molecular events between tumor and stromal TME cells that may affect ADC effects, still a major issue in clinical settings,[67] and partly driven by cancer-stromal crosstalk present in the TME.[1] ADC-resistant cancer cell lines[68,69] can be cultured in 3D spheroids along with TME components to study resistance mechanisms. Those resistance mechanisms that arise directly in cancer cells due to long-term exposure to mAbs can be influenced also by other TME components. In fact, it has been shown that CAFs derived from BC patient-derived tissues promote resistance to a HER2 inhibitor, lapatinib, in HER2+ BC cells.[70] In addition, TME-associated CAFs sustain chemoresistance in solid tumors.[71] Qualitative assessment of a fluorescent live/dead assay by fluorescence microscopy showed a general detrimental effect of ADCs upon tumor cell viability in culture. The quantitative LDH leakage analysis revealed a decrease in ADC-induced cell death in BC HCC1954 spheroids co-cultured with hFs, compared to spheroid monocultures, suggesting a degree of resistance to Tmab-ADCs. Loss of target expression is one of the mechanisms reported for acquired resistance against ADCs.[72] Still, our data showed that HER2 expression is maintained in HCC1954 HER2+ tumor spheroids, even in the presence of hFs. This suggests that loss of HER2 expression is not the mechanism behind such reduced sensitivity against ADCs in spheroids co-cultured with hFs. Nevertheless, further studies and conditions are required to fully understand the potential contribution of hFs in the model to sustain chemoresistance against Tmab-ADCs.

Increasing evidence has shown the potential of immunotherapy as an alternative approach to tackle BC.[4] The addition of an immune compartment to 3D cell models allows to study immunomodulatory events associated with those therapies. Herein, we co-cultured human naïve monocytes with spheroids from cell lines from different BC subtypes, under agitation. At day 7 of

Unst: $CD45^+/7AAD^-$ unstained samples. Histograms representing CD206 and CD163 MFI median fluorescent intensity are shown. Relative percentage of $DCSIGN^+/CSF1R^+$ (C) and $DC\text{-}SIGN^-/CSF1R^-$ (D) among $CD45^+/7AAD^-$ macrophages retrieved from MDA-MB-231 3D-3 cultures after challenge with DMSO, BLZ945, IgG and anti-CSF1R (α-CSF1R). Data were normalized to the values obtained in unchallenged condition (CNTR), set as 1 (dashed line). Data are shown as mean ±SD of n = 3 independent experiments. Statistic: two-tail Welch t-test (*: $p<0.05$; **: $p<0.001$). E) Relative CSF1R MFI in $CD45^+/7AAD^-$ macrophages (live cells) retrieved from MDA-MB-231 3D-3 cultures after exposure to DMSO, BLZ945, IgG and anti-CSF1R (α-CSF1R), normalized to those of unchallenged condition – control, CNTR), set as 1 (dashed line). Data are shown as mean ±SD of n = 3 independent experiments. Statistic: T-test with Welch correction (*: $p<0.05$). A representative CSF1R MFI plot is shown. F) Representative dot plots of $CD80^+CD86^+$ macrophages within $CD45^+/7AAD^-$ macrophages (live cells) retrieved from MDA-MB-231 3D-3 cultures after exposure to DMSO, BLZ945, IgG and anti-CSF1R (α-CSF1R). G) Relative percentage of $CD80^+CD86^+$ among $CD45^+/7AAD^-$macrophages retrieved from MDA-MB-231 3D-3 cultures after challenges with DMSO, BLZ945, IgG and anti-CSF1R (α-CSF1R). Data were normalized to the values obtained in unchallenged condition (CNTR), set as 1 (dashed line) Data are shown as mean ±SD of n = 3 independent experiments. Statistic: T-test with welch correction. ns: not significant; Unst: Unstained sample.

co-culture, the fraction of myeloid cells was significantly increased in HCC1954, HCC1806, and MDA-MB-231 co-cultures. These results recapitulate the higher macrophage infiltration reported in HER2+ and TNBC patients.[44,73] Further, myeloid cells in all BC co-cultures presented an immunosuppressive TAM phenotype, with a high fraction of cells positive for both CD206 and CD163. CD206 actively participates in homeostasis and macrophage activation, mediating the clearance of pathogens and proteins involved in inflammatory events.[74,75] The increased detection of CD206 in MDA-MB-231 co-cultures thus suggests higher activation of macrophages when cultured with this cell line. The higher myeloid population and immunosuppressive phenotypes observed in these co-cultures can be correlated with increased secretion of M-CSF and lactate, reported to modulate the TME towards an anti-inflammatory state.[47,76,77] These results highlight the potential of these cell models to study specific events leading to the establishment of an immunosuppressive TME landscape and to understand TAM immunosuppressive phenotype in the context of BC.[78]

We have added monocytes to hFs and CSF-1/M-CSF producing tumor spheroids of the MDA-MB-231 cell through our 3D-3 culture methodology to develop a more recapitulative TME, where most macrophages showed a TAM-like phenotype. This model was used to test the immunomodulatory potential of an anti-CSF1R blocking mAb. Challenging the 3D-3 cultures both with a CSF1R chemical inhibitor (BLZ945) and α-CSFR1 mAb resulted in downregulation of the expression of immunosuppressive genes, mainly *CD163, MRC1, DC-SIGN*, and *CSF1R*. Similar downregulation of anti-inflammatory genes was reported for an in vivo mouse model of glioblastoma (GBM) upon exposure to BLZ945.[79] Flow cytometry analysis revealed a decrease in the CSF1R$^+$/DC-SIGN$^+$ TAM subpopulation, especially after α-CSFR1 exposure. Contrarily, an increase in the CSF1R$^-$/DC-SIGN$^-$ cell subpopulation was observed, characterized by reduced levels of both CD163 and CD206. These results suggest an impairment in the differentiation of anti-inflammatory TAMs, induced by blockade of CSF1R.

The CSF1R inhibition-induced downregulation of DC-SIGN, a lectin highly expressed in TAMs,[61] is in agreement with a previous study in THP-1 cells.[80] The authors reported reduced DC-SIGN protein levels upon α-CSFR1 exposure.[80] Downregulation of CD163, CD206, and CD204 was also reported in tumor biopsies from a cohort of 31 patients (including 13 BC patients) treated with RG7155, a CSF1R-blocking mAb used in clinical studies.[13,81] CSF1R detection was drastically reduced in tumor tissue from patients exposed to α-CSF1R, an effect that we also observed in our challenged 3D-3 cultures. We showed that this effect is mediated by rapid internalization of the CSF1R-α-CSF1R complex, which occurred as soon as 3 h post mAb exposure, similar to what has been reported for other Abs.[82]

Upon CSF1R inhibition, we have not observed alterations in inflammatory markers, either at gene expression or at protein levels. These observations agree with data reported by Pyonteck and colleagues. In their GBM mouse model, CSF1R inhibition impaired the anti-inflammatory TAM phenotype of GBM-associated macrophages, while most inflammatory markers were not upregulated.[79] In contrast, Moughon and colleagues reported that, in ID8 and OVCAR3 ovarian cancer mouse models, exposure to another CSF1R inhibitor, GW2580, resulted in a marked increase of inflammatory macrophages in malignant ascites.[83] Such discrepancy can be explained by the distinct tumor TME scenarios, which may affect the general response against CSF1R modulating agents. The versatility of our 3D cell culture methodology to culture different cancer cell types (BC, lung cancer, sarcomas)[27–29], along with TME components will allow for ascertaining differential therapeutic response discrepancies under various TME scenarios. In addition, it will allow the testing of different therapies (e.g., chemotherapy,[84] immune checkpoint inhibitors)[10,14,85], thus assisting clinical and co-clinical studies. We envisage that this versatile methodology would be helpful defining in vitro therapeutical potential of various treatments by employing different cancer cell type-derived spheroids co-cultured with macrophages and fibroblasts.

A clear advantage of this methodology is its ability to sustain TAM differentiation from human primary monocytes.[86] TAMs are characterized by tremendous plasticity, enabling them to adapt quickly to differential microenvironmental conditions.[87] Several therapeutics have been developed to subvert the TAM phenotype, reshaping a more favorable immune TME to dampen BC.[88] Our 3D model will also allow the in-depth transcriptomic characterization (e.g., scRNAseq) of the various TAM sub-populations generated in different reconstructed TME and upon exposure to various stimuli (e.g., pro-inflammatory, immunomodulatory).[89] TNF-α challenge clearly induced inflammation in 3D-3 cultures and CSF1R inhibition dampened anti-inflammatory markers expression which proves that modulation of the overall TME status is possible in our model.

4. Conclusion

In conclusion, we provide a versatile 3D cell culture methodology, which allows the co-culture of various cancer cell types with different TME cell components. Nevertheless, it is important to point out that the model could still be improved by including other TME components, such as endothelial cells and other immune cells.[90] We have recently reported the co-culture of BC spheroids with PBMCs, namely to address the dynamics of the NK cell population upon antibody challenge.[30] The incorporation of additional TME components will be instrumental in taking full advantage of this methodology in disentangling the molecular interactions among TME components affecting therapeutic responses, including immunotherapeutic approaches.[88] Thus, we envisage future applications to 1) assess the potential of novel mAbs with different therapeutic modalities (e.g., bispecific, multimeric, immunomodulatory, stromal-directed ADCs[16,35,91] and 2) uncover and challenge the mechanisms behind tumor resistance to mAb-mediated therapies.[72] We also envision that, in the future, in-depth and high-content imaging analysis (namely, different quantitative automatized imaging techniques[92]), can be coupled to our TME-recapitulative cell culture methodology[93] for a more precise assessment of Ab therapeutic potential.

5. Experimental Section

2D Cell Culture: Cancer cell lines were acquired from ATCC. MCF-7 BC cell line was cultured in Dulbecco's Modified Eagle Medium (DMEM), high glucose, no phenol red, no glutamine, supplemented with 10% (v/v) Fetal

Bovine Serum (FBS), 2% (v/v) Glutamax and 1% (v/v) sodium pyruvate. SKBR-3 cell line was cultured in McCoy's 5A medium, supplemented with 10% (v/v) FBS. BT474, HCC1954, MDA-MB-231, and HCC1806 cell lines were cultured in Roswell Park Memorial Institute (RPMI 1640) medium, supplemented with 10% (v/v) Fetal Bovine Serum (FBS). The H157 lung cancer cell line was cultured in RPMI 1640 medium supplemented with 2 mM GlutaMAX, 10% (v/v) FBS, 12 mM HEPES, 1 mM sodium Pyruvate and 0.1 mM of non-essential amino acids. All supplements used for cell culture were purchased from Gibco. Cells were sub-cultured twice a week at the following seeding density: 25 000 cell cm^{-2} (BT474), 8 000 cell cm^{-2} (HCC1954), 15 000 cell cm^{-2} (MCF-7, MDA-MB-231 and HCC1806) or 10 000 cell cm^{-2} (SKBR-3 and H157). Human dermal fibroblasts (hFs, Innoprot) were cultured in Iscove's Modified Dulbecco's Medium (IMDM) supplemented with 10% (v/v) FBS. hFs were sub-cultured every 2 weeks, at a seeding density of 5 000 cells cm^{-2}. The medium was replaced every week. After thawing, cancer cell lines were sub-cultured at least twice before being used for aggregation or other assays. Both hFs and cancer cell line cultures were maintained in a humidified incubator at 37 °C and 5% CO_2.

Cancer Cell Aggregation: MCF-7, BT474, H157, and HCC1954 cells were inoculated in 125 mL spinner vessels (Corning), at a final cell density of 0.2×10^6 cells mL^{-1} and kept at 37 °C and 5% CO_2, according to previously established protocols.[29,32] Aggregation was induced at 80 rpm and cell lines were kept for 1 day for MCF-7 and BT474, 3 days for H157, and 4 days for HCC1954. For the remaining lines, cell aggregation was carried out for 3 days in Aggrewell 400 plates (Stemcell Technologies), with an inoculum of 500 cells/microwell, following the manufacturer's instructions. Spheroids were gently recovered from spinner vessels and Aggrewell plates for subsequent applications.

Human Peripheral Blood-Derived Monocyte Isolation: Human buffy coats were obtained from the Portuguese Blood Bank (i.e., Instituto Português do Sangue e Transplantação – IPST). Isolation of PBMCs from buffy coats and then monocytes from PBMCs was performed as reported previously.[29] Briefly, buffy coats were diluted in phosphate buffer saline (PBS) supplemented with 2% (v/v) FBS and 2 mM ethylenediaminetetraacetic acid (EDTA). Diluted buffy coats were processed by density centrifugation on Lymphoprep and peripheral blood-derived mononuclear cell (PBMCs) fraction was recovered. Subsequent washing steps were performed on PBMCs to minimize contamination with platelets and red blood cells. Monocytes were isolated through immunomagnetic negative selection, using the EasySep Human Monocyte Isolation Kit (Stemcell Technologies). Monocytes were used directly either for macrophage differentiation in 2D cultures or co-culture with cancer cell spheroids (to obtain TAMs) in alginate microcapsules, with or without hFs.[29]

Alginate Microencapsulation and 3D Cell Culture: Alginate microencapsulation of BC multicellular spheroids monocultures was performed using an electrostatic encapsulator (VarV1, Nisco) as previously described.[28,32] Briefly, BC spheroids were collected from spinner vessels or AggreWell 400 plates, counted, and 2×10^4 spheroids were washed with PBS 1X and resuspended in 1 mL of 1.1% (w/v) of Ultra-Pure Ca2+ MVG alginate (UP MVG NovaMatrix, Pronova Biomedical), prepared in sterile NaCl 0.9% (w/v). Resuspended cell spheroids were run through a nozzle with a diameter of 500 µm, charged at 5.3 kV, and collected into a 20 mM $BaCl_2$, 115 mM NaCl solution. For microencapsulation of cancer spheroids along with hFs and monocytes a nozzle of 700 µm was used, charged at 4.7 kV. Additionally, BC cells, hFs, and monocytes were in a 1:1 (BC + hFs co-cultures) 3:1 (BC + monocytes co-cultures) or 1:1:1 ratio (BC + hFs + monocytes triple co-cultures), per co-culture. Prior to encapsulation, hFs were stained with CellTrace Violet or Yellow and monocytes with CellTracker Deep Red (Invitrogen), according to the manufacturer's instruction, to identify both cell types in subsequent flow cytometry analysis and immunofluorescence (IF). Mono (BC spheroids), double (BC spheroids + hFs; BC spheroids + monocytes), and triple co-cultures (BC spheroids + hFs + monocytes) were kept in shake flasks with the appropriate medium for each cancer cell line, in a Multitron incubation shaker (INFORS HT) under 100 rpm continuous orbital agitation, at 37 °C, 5% CO_2. Half of the medium was replaced twice a week.

Immunofluorescence (IF) Microscopy: Alginate microcapsules were washed with PBS 1X and fixed for 20 min with 4% (v/v) paraformaldehyde (PFA) (Fluka) + 4% (v/v) sucrose (Sigma–Aldrich). Permeabilization/blocking was carried out by exposing fixed microcapsules to 1% (v/v) Triton X-100 (Sigma) with 0.2% (v/v) Fish Skin Gelatin (FSG, Sigma) in PBS 1X for 2 h at room temperature (RT). Samples were incubated with the primary Ab, anti-EGFR (Cell Signalling #D3B1; diluted 1/50), and anti-HER2 (Cell Signalling #29D8; diluted 1/100) in PBS 1X with 0.125% FSG, for 2 h at RT, followed by an overnight incubation at 4° C. Microcapsules were then washed and incubated for 1 h at RT with secondary Ab solution, diluted 1/500) in PBS 1X with 0.125% w/v FSG. To identify macrophages within co-cultures, either the signal from CellTracker Deep Red was used (BC spheroids + monocytes co-cultures) or samples were incubated with Alexa Fluor 488-conjugated anti-human CD45 (Biolegend, #304019; diluted 1/50) (3D-3 triple co-cultures). Microcapsules were then washed with PBS 1X, counterstained with 4′,6-diamidino-2-phenylindole (DAPI) or DRAQ5 (both from ThermoFisher) for nuclei identification, washed again and mounted in Prolong Gold antifade (Life Technologies). For BC + hFs and 3D-3 cultures, samples were visualized using a confocal microscope (LSM880 with Fast Airyscan, Zeiss), and maximal projections of 1 µm Z-stack images were analyzed on ImageJ (Fiji). 2D cultures of hFs and HCC1954 were washed with PBS 1X, fixed for 10 min at RT with 4% (v/v) paraformaldehyde (PFA) (Fluka) + 4% (v/v) sucrose (Sigma-Aldrich), and blocked/permeabilized for 20 min with 0.2% (w/v) FSG in PBS with 0.1% TritonX-100. hFs were incubated overnight with anti-HER2 diluted 1/200 in 0.125% FSG solution. Cells were then washed and incubated for 1 h with a secondary Ab (conjugated with Alexa Fluor 488 (Invitrogen), diluted 1/500) solution, prepared in 0.2% w v^{-1} FSG in PBS. Samples were mounted in Prolong Gold antifade (Life Technologies) and counterstained with 4′,6-diamidino-2-phenylindole (DAPI) for nuclei identification. Samples were visualized using a widefield fluorescence microscope (DMI6000, Leica) and analyzed on ImageJ (Fiji).

Antibody-Drug Conjugates (ADCs) Synthesis and Production: A set of Tmab-based anti-HER2 Antibody Drug Conjugates (ADCs) were synthesized and produced in HEK293 cells, following an established methodology.[36] Tmab complete amino acid sequence was retrieved from the DrugBank database.[94] Antibodies were conjugated to either DM1 (Mertansine) or MMAE (Monomethyl Auristatin E) employing two chemical conjugation strategies (heterogeneous and homogeneous[36]), resulting in distinct IgG molecular species with different drug-antibody-ratios (DAR): heterogeneous conjugated Tmab-DM1 (KADCYLA Biosimilar, DAR 3.1), heterogeneous conjugated Tmab-MMAE4 (DAR 4), homogeneous conjugated Tmab-MMAE8 (DAR 8) and homogeneous conjugated Tmab-Cys114-MMAE2 (DAR 2). Unconjugated control Tmab and Tmab-Cys114 (a genetically modified antibody (thiomab) with substituted alanine for cysteine at position 114 that allows for site-directed conjugation) were used in parallel as control for conjugated antibodies (Tmab for Tmab-MMAE4, Tmab-MMAE8, Tmab-DM1 and Tmab-Cys114 for Tmab-Cys114-MMAE2). Antibodies solutions were filtered through an Acrodisc Syringe Filter Low Protein Binding 0.2 µm Supor Membrane (Pall Corporation) and stored at +4 °C. ADCs were also analysed by SDS-PAGE, performed in NuPAGE 4–12% Bis-Tris Gel (Invitrogen), 1 µg/lane, both in the reducing and non-reducing conditions (the former achieved by boiling the samples at 95 °C in the presence of 1X NuPAGE Reducing Buffer, Invitrogen). ADC samples were loaded in NuPAGE Loading Buffer (Invitrogen). A molecular weight control standard was run in parallel (Precision Plus Protein All Blue Prestained Protein Standards, Biorad). Protein bands were visualized by InstantBlue Comassie-based staining solution (Sigma) in an iBright FL1500 Imaging system (Invitrogen). Detailed ADC descriptions were provided in Table 1. Details on cloning strategy, production, and characterization of the ADCs performed by high-performance liquid chromatography-hydrophobic interaction chromatography (HPLC-HIC), mass spectrometry (MS), and UV spectroscopy are available in Supporting Information and Experimental Section.

Effect of ADCs on Metabolic and Cell Viability in 2D Cell Cultures: HER2+ HCC1954 cells were plated at 3000 cells/well in quadruplicates in 96-well tissue culture plates, in 100 µL culture medium per well, and cultured in a humidified incubator at 37 °C and 5% CO_2. After 24 h, cells

were challenged with 100 µL of fresh culture medium containing serial dilutions of the ADCs (final concentrations 0.001–10 µg mL^{-1}, corresponding respectively to 0.00673 nM and 67.38 nM). Cellular metabolic activity was assessed immediately after plating and at the end of the ADCs challenge by measurement of the resazurin reduction activity employing the PrestoBlue assay (Invitrogen), according to the manufacturer's instructions. The mean fluorescence of the reagent was subtracted from each replicate and condition, and the mean value of each condition was normalized by day 0 (before ADCs challenge). Metabolic activity was represented as a percentage relative to ADC-vehicle condition (control, CNTR). Cell viability was assessed at the end of the ADCs challenge employing the crystal violet assay. Briefly, after exposure to ADCs, the medium was removed, and cells were fixed in Formalin Solution 10% Neutral Buffered (Sigma–Aldrich) for 10 min at room temperature, washed with PBS, and stained with 10% crystal violet (w/v) (Merck) in 20% methanol (v/v) for 20 min under orbital agitation. The excess dye was removed by repeated washes with distilled H_2O. After complete water removal and drying, crystal violet crystals were dissolved in 10% (v/v) glacial acetic acid (Merck) under orbital agitation, for 20 min. Absorbance was measured at 595 nm, in an Infinite 200 PRO NanoQuant plate reader (TECAN). Cell viability was represented as a fold change relative to CNTR.

ADCs Challenge and Cytotoxicity Analysis in Encapsulated 3D Cell Cultures: BT474 and HCC1954 cultures (mono- and co-cultures with hFs) were kept for 1 week in culture post-encapsulation in a Multitron INFORS HT shaker under continuous agitation (100 rpm orbital agitation, at 37 °C, 5% CO_2). Then, microcapsules were seeded in quadruplicate in 96-flat bottom well plates (20–30 cells/well) and exposed to 1/5 serial dilutions of Tmab_cys114-MMAE2 in culture medium (0.001 to 10 µg mL^{-1}, corresponding respectively from 0.00673 to 67.38 nM) at 37 °C and 5% CO_2. In addition, alginate microcapsules containing HCC1954 mono- and co-cultures with hFs were exposed in parallel to different ADCs at 33 nM, which was expected to exert cytotoxic effects. Twice a week, half of the spent medium was removed and replaced with fresh culture medium supplemented with ADCs. To evaluate cell cytotoxicity, a commercial LDH release assay was employed (CyQUANT LDH Cytotoxicity Assay, Invitrogen). Results represent n = 3 biological replicates. The percentage of drug-induced cell death was determined as in[38] (formula 5: [1 − (***lysate LDH treated***÷***lysate LDH control***)] × 100) and shown as the percentage of ADC-induced cell death compared to the ADC vehicle control condition (CNTR). Relative EC50 was evaluated at 2 weeks post-exposure, in agitated cultures as above.

Cell Viability Assessment in 3D Cell Cultures: Microcapsules were incubated for 5 min with 5 µg mL^{-1} Fluorescein Diacetate, FDA (Sigma-Aldrich) and 1 µM TO-Pro-3 (Invitrogen) or 1 h with 50 nM Calcein-AM (Corning) and 10 µg mL^{-1} propidium iodide (PI) and observed in a widefield (DMI6000, Leica) or confocal microscope (MICA, Leica). Cells that accumulated the fluorescent byproduct from FDA or Calcein-AM metabolization were considered alive, while cells positive for cell membrane impermeant dyes TO-Pro-3 or PI were considered dead. Intensity levels for FDA and TO-Pro-3 signal were further evaluated in HCC1954 mono- and co-cultures with hFs, after challenge with Tmab_cys114-MMAE2 and the respective Ab control. For cell viability assessment in de-encapsulated cultures, after 2 weeks of challenge, microcapsules were washed with PBS 1X and dissolved by using a chelating solution (10 mM HEPES pH 7.4, 100 mM EDTA). After chelation, released spheroids were exposed to a mixture of FDA and TO-Pro-3, for 2 min at room temperature and pictures were taken either by widefield or confocal microscopy. To avoid FDA signal saturation, photos were acquired after exposing each de-encapsulated culture to the FDA/TO-Pro-3 solution, keeping a constant laser exposure across samples. Background fluorescent intensity was subtracted in each photo, and the FDA/TO-Pro-3 intensity ratio was evaluated through the ICY Software and shown as the mean FDA/TO-Pro-3 intensity ratio for each spheroid analyzed. As a positive control for cell death, HCC1954 mono- and co-cultures with hFs, were exposed for 2 weeks to 100 nM DM1 (Mertansine, cytotoxic drug, Abcam #146096), prepared in N, N-Dimethylacetamide, 99% (Alfa Aesar, Thermo Fisher). The challenge was performed under continuous agitation, in a Multitron INFORS HT shaker (100 rpm orbital agitation, at 37 °C, 5% CO2). Twice a week, half of the spent medium was removed and replaced with fresh culture medium supplemented with DM1. The non-parametric Kruskal-Wallis test, followed by Dunn's multiple comparisons, was performed for statistical analysis.

Protein Extraction: BT474 and HCC1954 encapsulated spheroids were collected 1- and 2-weeks post-encapsulation. Alginate microcapsules were washed with cold PBS and chelated as described above. Released 3D spheroids were centrifuged at 100 xg for 5 min and the pellets were incubated in RIPA 1X buffer (Millipore), supplemented with protease and phosphatase inhibitors (Roche), for 1 h on ice. The resulting cell lysates were centrifuged at 13 000 xg (4 °C) and the supernatant was transferred to pre-cooled plastic tubes.

Cancer cell spheroids and hFs suspensions were filtered through a 40 µm strainer prior to lysis, to separate 3D spheroids from hFs. Retained 3D spheroids were washed 3 times with cold PBS, recovered from the strainer, centrifuged, lysed, and processed as described above. HCC1954 and hFs growing in 2D were washed with cold PBS and lysed directly with RIPA buffer. Samples were quantified by Pierce BCA Protein Assay Kit (Thermo Fisher), according to the manufacturer's instructions, and stored at −80 °C. Protein samples for SDS-PAGE were prepared with NuPAGE LDS Sample Buffer (Invitrogen) and NuPAGE Sample Reducing Agent (Invitrogen), both added at 1X final concentration.

Western Blot Analysis: Samples were heated at 70 °C for 10 min, continuously sonicated for 2 min, and loaded onto NuPAGE 4–12% Bis-Tris Gel (Invitrogen). SDS-PAGE was conducted at 150 V for 1.5 h, followed by electroblotting of proteins by wet transfer onto Polyvinylidene fluoride (PVDF) membranes at 20 V, for 1 h, using a Mini Blot Module (Invitrogen). Membranes were blocked in 5% (w/v) skimmed milk in 1X TBST (Cell Signalling) and incubated overnight under agitation with the following primary antibodies and dilutions: anti-HER2 (#29D8, Cell Signalling; 1/2000); anti-E-cadherin (#B610181, BD; 1/1000), anti-CD90 (#7E1B11, Abcam; 1/1000). Anti-β-actin antibody (#A5441, Sigma; 1/5000) was used as a loading control. After washing with 1X TBST, membranes were incubated for 1 h at RT with the appropriate secondary antibodies, conjugated with Horseradish Peroxidase (HRP): goat anti-mouse IgG-HRP, (#A2554; 1/5000) or goat anti-rabbit IgG-HRP (#A0545; 1/5000), both from Sigma–Aldrich. Membranes were developed using Amersham ECL Select Western Blot Detection Reagent (GE Healthcare) and visualized using an iBright FL1500 Imaging system (Invitrogen).

Macrophage Differentiation from Monocytes and Challenge in 2D Cultures: To induce macrophage differentiation, monocytes isolated from healthy donor PBMCs were cultured in 96-well cell culture plates at a seeding density of 9.6 × 10^4 cells/well or in 12-well cell culture plates at 2 × 10^6 cells/well. Monocytes were kept in RPMI 1640 medium supplemented with 10% FBS (v/v), 1% (v/v) penicillin/streptomycin (Life Technologies) and 50 ng mL^{-1} macrophage colony-stimulating factor (M-CSF; PeproTech), for 6 days at 37 °C and 5% CO_2. Then, macrophages were exposed for 2 days to 20 ng mL^{-1} of both IL-4 and IL-13 (PeproTech) and subsequently challenged for 2 days with BLZ945 (1 µM, Selleckchem), its vehicle, DMSO (Sigma, 0.001% v/v), an α-CSFR1 blocking antibody (0.5 µg mL^{-1}, anti-CSFR1, IgG1 MAB3291-100, R&D System), and a mouse IgG1 isotype control (0.5 µg mL^{-1}, IgG1, MAB002, R&D System). After the challenge, cell viability was analyzed by PrestoBlue reduction assay (Invitrogen) and crystal violet assay, following the procedures described above. Results represent 3 biological replicates and were shown as fold change in cell and metabolic viability for each condition compared to the unchallenged condition (control, CNTR). Statistical analysis was performed by the Kruskal–Wallis test, followed by Dunn's correction test for multiple comparisons, comparing each condition to CNTR.

Competition Assay and α-CSF1R Internalization in 2D Cultures of Macrophages: For the competition assay between the blocking and staining Ab's against CSFR1, monocyte-derived macrophages were harvested with a cold 10 mM EDTA solution, centrifuged at 400 xg for 10 min and the Fc receptor was blocked by using Human TruStain FcX for 30 min at 4 °C in flow cytometry (FC) buffer (PBS 1X with 2% FBS (v/v)). Macrophages were washed in FC buffer and stained for 30 min at 4 °C with the following Ab combinations and conditions: 1) anti-CSF1R conjugated with Brilliant Violet 711 (BV711) dye (#3347318, Biolegend) alone; 2) anti-CSFR1 blocking Ab (0.5 µg mL^{-1}, α-CSF1R, IgG1, MAB3291-100, RD System)

alone; 3) co-incubation of anti-CSF1R-BV711 and α-CSF1R blocking antibody; 4) pre-incubation (30 min) with anti-CSF1R blocking Ab, followed by washing and incubation with anti-CSF1R-BV711. All Ab mixtures were prepared in FC buffer, at 4 °C. Challenged macrophages were washed and further stained with secondary goat anti-mouse Alexa-Fluor 488 (Invitrogen), diluted 1/2000 in FC buffer for 40 min at 4 °C for the detection of the α-CSF1R blocking Ab. For measurement of α-CSFR1 internalization, monocyte-derived macrophages were exposed for 0, 1.5, 3, 18, 48, or 72 h to 0.5 µg mL^{-1} of α-CSFR1 blocking Ab and harvested as above. CSF1R binding at the cell surface was detected by incubating macrophages with a secondary goat anti-mouse Alexa Fluor 488 antibody (Invitrogen), at a 1/2000 dilution in FC buffer, for 40 min on ice. Macrophages exposed only to the secondary Ab were included as controls. FC was performed in a FACSCelesta Cell Analyzer (BD). DAPI (Invitrogen) was used for the exclusion of dead cells. Data was analyzed in the FlowJo software (version 10). Results were shown as the mean and standard deviation of 4 biological replicates and represent the median fluorescence intensity (MFI) for the Alexa Fluor 488 or BV711 channels, expressed in arbitrary units. Statistical analysis was performed by the Kruskal–Wallis test, followed by Dunn's correction test for multiple comparisons.

CSF1R Inhibition in MDA-MB-231 3D-3 Cultures: At 4 days post-encapsulation, 3D heterotypic cultures of MDA-MB-231 spheroids, hFs and macrophages were challenged for 3 days with BLZ945 (1 µM), DMSO (BLZ945 vehicle, 0.0001% v/v), α-CSF1R or the isotype IgG (both at 0.5 µg mL^{-1}) in a Multitron incubation shaker (INFORS HT) under continuous orbital agitation of 100 rpm, at 37 °C, 5% CO_2. Cells were recovered for flow cytometry and gene expression analysis by RT-qPCR. The cell supernatant was collected for ELISA assays as described below.

3D-3 Cultures Exposure to TNF-α: To induce inflammation in 3D-3 H157 and HCC1806 cultures, microcapsules were plated in triplicate in ultra-low attachment (ULA) plates (Corning) in the respective medium and challenged with 10 ng mL^{-1} TNF-α (PeproTech) for 3 days, under continuous orbital agitation. After the challenge, the culture supernatant was centrifuged at 14 000 xg at °4 C for 10 min to eliminate cell debris, snap-frozen, and stored at −80 °C until analysis.

Flow Cytometry Macrophage Phenotype Analysis in Heterotypic Co-cultures: Alginate microcapsules from double (BC spheroids + monocytes) and 3D-3 cultures were chelated and centrifuged at 100 xg, for 2 min to separate single cells from the spheroid fraction. Single-cell suspension comprising mainly hFs and macrophages was recovered to a separate tube. The MDA-MB-231 spheroid fraction was incubated with TrypLE Select Enzyme (1X) (Gibco) for 5 min, at 37 °C, to obtain a single-cell suspension. Cells from both fractions were pooled and centrifuged at 400 xg, for 10 min, followed by incubation with Abs mixtures, diluted in FC buffer for 40 min on ice. The following Abs (all from Biolegend) were used: anti-CD45 conjugated with Allophycocyanin (APC), anti-CD45-APC (#555483), anti-CD206-AF488 (#321114), anti-CD163-Phycoerythrin (PE) (#326506), anti-DC-SIGN-PE-Cyanine 7 (Cy7) (#3330113), anti-CSF1R-BV711 (#3347318), anti-CD80-PE (#305220), anti-CD86-AF488 (#305413). Cells were then washed in FC buffer and analyzed in a FACSCelesta Cell Analyzer (BD). 7-Aminoactinomycin D (7-AAD) (#420404, Biolegend) was used for the exclusion of dead cells. Results were analyzed in the FlowJo software (version 10). The gating strategies for the analysis are shown in Experimental Section and Figures S2 and S3 (Supporting Information). Results represent at least 3 biological replicates and were shown as fold change compared to the control condition. Statistical analysis was performed by T-test with Welch's correction test, followed by Tukey's test for multiple comparisons.

Cytokine Screening by Antibody Arrays: The medium from double co-cultures of BC spheroids and monocytes was collected at day 7 post-encapsulation, centrifuged at 1000 xg for 10 min at 4 °C, snap freeze in liquid nitrogen, and stored at −80 °C until analysis. Processed media was analyzed using the Human Cytokine Antibody Array (#ab133998, Abcam), according to the manufacturer's procedure. Samples were left to incubate overnight, at 4 °C. Membranes were developed in ChemiDoc (Bio-Rad), and the images were treated on Image Lab (Bio-Rad). Each dot density was calculated using the software's densitometry tools. To compare between samples, an intensity correction factor was calculated by dividing the positive controls of each membrane by the positive control of a selected membrane. The correction factor was then applied to the spots of all membranes, normalizing samples to the same positive control. Results represent 3 biological replicates and were shown as mean cytokine concentration and standard deviation. Statistical analysis was performed by One-way ANOVA, followed by Tukey's test for multiple comparisons.

Cytokine Secretion Analysis by ELISA: The concentration of M-CSF (BC spheroids + monocytes co-cultures) and IL-8/CXCL8 and CCL5/RANTES (3D-3 cultures) was measured in cell culture supernatants using Quantikine ELISA kits (R&D Systems, #DMC00B, #D8000C, and #DRN00B, respectively), following the manufacturer's instructions. Samples were analyzed in duplicate, and absorbance was measured at 450 and 540 nm in an Infinite 200 PRO NanoQuant plate reader (TECAN). Data was shown as mean ng/mL (BC spheroids + monocytes) or pg mL^{-1} (3D-3 cultures) of secreted cytokine and SD from at least 2 independent assays. Statistical analysis was performed by One-way ANOVA, followed by Tukey's test for multiple comparisons.

Lactate Secretion Analysis: The medium from double co-cultures (BC spheroids + monocytes) was processed and stored as mentioned above. Lactate concentration in the media was analyzed with Cedex Bio Analyzer (Roche Custom Biotech), following the manufacturer's instructions.

RNA Extraction and RT-qPCR Analysis: RNA from 3D co-cultures was extracted with a High Pure RNA Isolation Kit (Roche) and cDNA synthesis was performed with the Sensiscript RT kit (Qiagen, #205213) following the manufacturer's instructions. RT-qPCR was performed with SYBR-Green (SYBR Green I Master Kit, Roche), in a LightCycler 480 equipment (Roche). Samples were run in triplicate and gene expression was determined through the comparative CT method ($2^{-\Delta\Delta CT}$),[95] using *CD68* gene expression as housekeeping control and employing the LightCycler480 software for analysis. Results represent 5 biological replicates analyzed in triplicate and were shown as fold change compared to the control condition (CNTR, unchallenged). The non-parametric Mann-Whitney test was performed for statistical analysis. Primer sequences used in this study are listed in Table S3 (Supporting Information).

Statistical Analysis: Statistical analysis was performed by Graph Pad Prisms software (version 10.2.1 for Windows) and assessed for at least three independent biological replicates. A p-value below 0.05 (*$p<0.05$); was considered throughout the manuscript as a threshold to indicate statistical significance. In the case of ADCs or mAb exposure, unchallenged samples were considered as control (CNTR) in all cases. Each set of data generated in biological replicates of Figure 5 was normalized to the CNTR before performing statistical analysis. Data were always shown as a mean value; error bars in the graphs represent standard deviation. For multiple comparisons, analysis was performed by One- or Two-Way Anova and non-parametric Kruskal Wallis test, followed by Dunn's correction. To compare two groups, a two-tailed T-test with Welch correction or Mann-Whitney were employed.

Supporting Information

Supporting Information is available from the Wiley Online Library or from the author.

Acknowledgements

G.D. and N.F.L. contributed equally to this work and share co-first authorship. The authors acknowledge funding from the Fundação para a Ciência e a Tecnologia/ Ministério da Ciência, Tecnologia e Ensino Superior (FCT/MCTES, Portugal) through national funds to iNOVA4Health (UIDB/04462/2020 and UIDP/04462/2020), the Associate Laboratory LS4FUTURE (LA/P/0087/2020), the grant PTDC/BTM-TEC/0432/2021 and the PhD scholarships 2020.07623.BD to NL, 2022.11642.BD to GT, and 2022.12962.BD to IRG. The authors also acknowledge funding from iBET (iBETXplore Starting grant; PI-3D-Abc-717). The authors thank Dr. Gabriela Silva for her critical review of the manuscript and fruitful scientific discussion.

Conflict of Interest

The authors declare no conflict of interest.

Data Availability Statement

The data that support the findings of this study are available from the corresponding author upon reasonable request.

Keywords

3D cancer models, antibody-drug conjugates, cancer-associated fibroblasts, targeted therapies, tumor-associated macrophages

Received: July 23, 2024
Revised: October 21, 2024
Published online: November 27, 2024

[1] M. R. Junttila, F. J. de Sauvage, *Nature* **2013**, *501*, 346.
[2] A. Tiwari, R. Trivedi, S. Y. Lin, *J. Biomed. Sci.* **2022**, *29*, 83.
[3] F. Anari, C. Ramamurthy, M. Zibelman, *Futur. Oncol.* **2018**, *14*, 1409.
[4] F. Ye, S. Dewanjee, Y. Li, N. K. Jha, Z. S. Chen, A. Kumar, Vishakha, T. B., S. K. Jha, H. Tang, *Mol. Cancer* **2023**, *22*, 105.
[5] B. R. Halle, D. B. Johnson, *Curr. Treat. Options Oncol.* **2021**, *22*, 30.
[6] V. Subbiah, C. Baik, J. M. Kirkwood, *Trends Cancer* **2020**, *6*, 797.
[7] F. Ye, S. Dewanjee, Y. Li, N. Kumar Jha, Z.-S. Chen, A. Kumar, T. Behl, S. Kumar Jha, H. Tang, S. Kumar Jha Saurabhjha, S. H. Tang, *Mol. Cancer* **2023**, *22*, 105.
[8] A. Behl, Z. A. Wani, N. N. Das, V. S. Parmar, C. Len, S. Malhotra, A. K. Chhillar, *Crit. Rev. Oncol. Hematol.* **2023**, *183*, 103915.
[9] S. Maximiano, P. Magalhães, M. P. Guerreiro, M. Morgado, *BioDrugs* **2016**, *30*, 75.
[10] S. Qin, L. Xu, M. Yi, S. Yu, K. Wu, S. Luo, *Mol. Cancer* **2019**, *18*, 155.
[11] T. N. J. Bullock, *Cell. Mol. Immunol.* **2021**, *19*, 14.
[12] X. Cao, Y. Wang, W. Zhang, X. Zhong, E. G. Gunes, J. Dang, J. Wang, A. L. Epstein, C. Querfeld, Z. Sun, S. T. Rosen, M. Feng, *Blood* **2022**, *139*, 3290.
[13] L. P. Pradel, C. H. Ooi, S. Romagnoli, M. A. Cannarile, H. Sade, D. Reuttinger, C. H. Ries, *Mol. Cancer Ther.* **2016**, *15*, 3077.
[14] S. F. Magkouta, P. C. Vaitsi, A. G. Pappas, M. Iliopoulou, C. N. Kosti, K. Psarra, I. T. Kalomenidis, *Cancers (Basel)* **2021**, *13*, 2546.
[15] Y. Y. Syed, *Drugs* **2020**, *80*, 1019.
[16] C. Peters, S. Brown, *Biosci. Rep.* **2015**, *35*, e00225.
[17] S. Menon, S. Parakh, A. M. Scott, H. K. Gan, *Explor. Target. anti-tumor Ther.* **2022**, *3*, 252.
[18] A. Q. Dean, S. Luo, J. D. Twomey, B. Zhang, *mAbs* **2021**, *13*, 1951427.
[19] K. Harper, *Cancer Discov.* **2019**, *9*, 158.
[20] G. von Minckwitz, C.-S. Huang, M. S. Mano, S. Loibl, E. P. Mamounas, M. Untch, N. Wolmark, P. Rastogi, A. Schneeweiss, A. Redondo, H. H. Fischer, W. Jacot, A. K. Conlin, C. Arce-Salinas, I. L. Wapnir, C. Jackisch, M. P. DiGiovanna, P. A. Fasching, J. P. Crown, P. Wülfing, Z. Shao, E. Rota Caremoli, H. Wu, L. H. Lam, D. Tesarowski, M. Smitt, H. Douthwaite, S. M. Singel, C. E. Geyer, *N. Engl. J. Med.* **2019**, *380*, 617.
[21] J. Cortés, S.-B. Kim, W.-P. Chung, S.-A. Im, Y. H. Park, R. Hegg, M. H. Kim, L.-M. Tseng, V. Petry, C.-F. Chung, H. Iwata, E. Hamilton, G. Curigliano, B. Xu, C.-S. Huang, J. H. Kim, J. W. Y. Chiu, J. L. Pedrini, C. Lee, Y. Liu, J. Cathcart, E. Bako, S. Verma, S. A. Hurvitz, *N. Engl. J. Med.* **2022**, *386*, 1143.
[22] R. M. Hoffmann, S. Mele, A. Cheung, D. Larcombe-Young, G. Bucaite, E. Sachouli, I. Zlatareva, H. O. J. Morad, R. Marlow, J. M. McDonnell, M. Figini, K. E. Lacy, A. J. N. Tutt, J. F. Spicer, D. E. Thurston, S. N. Karagiannis, S. Crescioli, *Sci. Reports* **2020**, *10*, 8869.
[23] M. Magzoub, S. Jin, A. S. Verkman, *FASEB J. • Res. Commun.* **2008**, *22*, 276.
[24] C. Jensen, Y. Teng, *Front. Mol. Biosci.* **2020**, *7*, 33.
[25] H. H. Tsai, K. C. Yang, M. H. Wu, J. C. Chen, C. L. Tseng, *Int. J. Mol. Sci.* **2019**, *20*, 4024.
[26] T. Franchi-Mendes, N. Lopes, C. Brito, *Front. Bioeng. Biotechnol.* **2021**, *9*, 649949.
[27] G. Domenici, R. Eduardo, H. Castillo-Ecija, G. Orive, Á. M. Carcaboso, C. Brito, *Cancers (Basel)* **2021**, *13*, 879.
[28] M. F. Estrada, S. P. Rebelo, E. J. Davies, M. T. Pinto, H. Pereira, V. E. Santo, M. J. Smalley, S. T. Barry, E. J. Gualda, P. M. Alves, E. Anderson, C. Brito, *Biomaterials* **2016**, *78*, 50.
[29] S. P. Rebelo, C. Pinto, T. R. Martins, N. Harrer, M. F. Estrada, P. Loza-Alvarez, J. Cabeçadas, P. M. Alves, E. J. Gualda, W. Sommergruber, C. Brito, *Biomaterials* **2018**, *163*, 185.
[30] S. Batalha, C. M. Gomes, C. Brito, *Front. Immunol.* **2023**, *14*, 1267621.
[31] S. Zwicker, D. Bureik, M. Bosma, G. L. Martinez, S. Almer, E. A. Boström, *PLoS One* **2016**, *11*, e0167324.
[32] V. E. Santo, M. F. Estrada, S. P. Rebelo, S. Abreu, I. Silva, C. Pinto, S. C. Veloso, A. T. Serra, E. Boghaert, P. M. Alves, C. Brito, *J. Biotechnol.* **2016**, *221*, 118.
[33] A. Chakrabarty, N. E. Bhola, C. Sutton, R. Ghosh, M. G. Kuba, B. Dave, J. C. Chang, C. L. Arteaga, *Cancer Res.* **2013**, *73*, 1190.
[34] X. Yao, J. Jiang, X. Wang, C. Huang, D. Li, K. Xie, Q. Xu, H. Li, Z. Li, L. Lou, J. Fang, *Preclinical Study* **2015**, *153*, 123.
[35] C. Szot, S. Saha, X. M. Zhang, Z. Zhu, M. B. Hilton, K. Morris, S. Seaman, J. M. Dunleavey, K. S. Hsu, G. J. Yu, H. Morris, D. A. Swing, D. C. Haines, Y. Wang, J. Hwang, Y. Feng, D. Welsch, G. DeCrescenzo, A. Chaudhary, E. Zudaire, D. S. Dimitrov, B. St. Croix, *J. Clin. Invest.* **2018**, *128*, 2927.
[36] M. Farràs, J. Miret, M. Camps, R. Román, Ó. Martínez, X. Pujol, S. Erb, A. Ehkirch, S. Cianferani, A. Casablancas, J. J. Cairó, *mAbs* **2020**, *12*, 1702262.
[37] J. Ou, Y. Si, K. Goh, N. Yasui, Y. Guo, J. Song, L. Wang, R. Jaskula-Sztul, J. Fan, L. Zhou, R. Liu, X. Liu, *PLoS One* **2018**, *13*, e0206246.
[38] M. C. Cox, R. Mendes, F. Silva, T. F. Mendes, A. Zelaya-Lazo, K. Halwachs, J. J. Purkal, I. A. Isidro, A. Félix, E. R. Boghaert, C. Brito, *Sci. Rep.* **2021**, *11*, 18571.
[39] L. Kisselbach, M. Merges, A. Bossie, A. Boyd, *Cytotechnology* **2009**, *59*, 31.
[40] D. Cretella, F. Saccani, F. Quaini, C. Frati, C. Lagrasta, M. Bonelli, C. Caffarra, A. Cavazzoni, C. Fumarola, M. Galetti, S. La Monica, L. Ampollini, M. Tiseo, A. Ardizzoni, P. G. Petronini, R. R. Alfieri, *Mol. Cancer* **2014**, *13*, 143.
[41] E. Giordani, M. Allegretti, A. Sinibaldi, F. Michelotti, G. Ferretti, E. Ricciardi, G. Zicchedda, F. Valenti, S. Di Martino, C. Ercolani, D. Giannarelli, G. Arpino, S. Gori, C. Omarini, A. Zambelli, E. Bria, I. Paris, S. Buglioni, P. Giacomini, A. Fabi, *J. Exp. Clin. Cancer Res.* **2024**, *43*, 182.
[42] J. Kao, K. Salari, M. Bocanegra, Y.-L. Choi, L. Girard, J. Gandhi, K. A. Kwei, T. Hernandez-Boussard, P. Wang, A. F. Gazdar, J. D. Minna, J. R. Pollack, *PloS one* **2009**, *4*, e6146.
[43] A. Rheinländer, B. Schraven, U. Bommhardt, *Immunol. Lett.* **2018**, *196*, 22.
[44] A. Mantovani, P. Allavena, F. Marchesi, C. Garlanda, *Nat. Rev. Drug Discovery* **2022**, *21*, 799.
[45] C. S. Subauste, R. de Waal Malefyt, F. Fuh, *J. Immunol.* **1998**, *160*, 1831.
[46] L. Cassetta, J. W. Pollard, *Nat. Rev. Drug Discovery* **2018**, *17*, 887.
[47] O. R. Colegio, N.-Q. Chu, A. L. Szabo, T. Chu, A. M. Rhebergen, V. Jairam, N. Cyrus, C. E. Brokowski, S. C. Eisenbarth, G. M. Phillips, G. W. Cline, A. J. Phillips, R. Medzhitov, *Nature* **2014**, *513*, 559.

[48] J. Deng, R. Jiang, E. Meng, H. Wu, *Front. Oncol.* **2022**, *12*, 944494.
[49] D. G. DeNardo, B. Ruffell, *Nat. Rev. Immunol.* **2019**, *19*, 369.
[50] N. Wang, W. Liu, Y. Zheng, S. Wang, B. Yang, M. Li, J. Song, F. Zhang, X. Zhang, Q. Wang, Z. Wang, *Cell Death Dis.* **2018**, *99*, 880.
[51] L. Albonici, M. G. Giganti, A. Modesti, V. Manzari, R. Bei, *Int. J. Mol. Sci.* **2019**, *20*, 2970.
[52] N. Lopes, V. G. Correia, A. S. Palma, C. Brito, *Int. J. Mol. Sci.* **2021**, *22*, 1972.
[53] L. Cassetta, J. W. Pollard, *Nat. Rev. Drug Discovery* **2018**, *17*, 887.
[54] X. Qiu, T. Zhao, R. Luo, R. Qiu, Z. Li, *Front. Oncol.* **2022**, *12*, 396.
[55] M. A. Cannarile, M. Weisser, W. Jacob, A. M. Jegg, C. H. Ries, D. Rüttinger, *J. Immunother. cancer* **2017**, *5*, 1.
[56] M. Jaguin, N. Houlbert, O. Fardel, V. Lecureur, *Cell. Immunol.* **2013**, *281*, 51.
[57] K. Xie, *Cytokine Growth Factor Rev.* **2001**, *12*, 375.
[58] F. Hirano, A. Kobayashi, I. Makino, *Int. Immunopharmacol.* **2003**, *3*, 225.
[59] J. Ding, C. Guo, P. Hu, J. Chen, Q. Liu, X. Wu, Y. Cao, J. Wu, *Int. J. Oncol.* **2016**, *49*, 2064.
[60] S. D. Jayasingam, M. Citartan, T. H. Thang, A. A. Mat Zin, K. C. Ang, E. S. Ch'ng, *Front. Oncol.* **2020**, *9*, 1512.
[61] B. Hu, Z. Wang, H. Zeng, Y. Qi, Y. Chen, T. Wang, J. Wang, Y. Chang, Q. Bai, Y. Xia, Y. Wang, L. Liu, Y. Zhu, B. Dai, J. Guo, L. Xu, W. Zhang, J. Xu, *Cancer Res.* **2020**, *80*, 1707.
[62] K. S. Purrington, J. Knight, G. Dyson, R. Ali-Fehmi, A. G. Schwartz, J. L. Boerner, S. Bandyopadhyay, *PLoS One* **2020**, *15*, e0231712.
[63] M. D. Burstein, A. Tsimelzon, G. M. Poage, K. R. Covington, A. Contreras, S. A. W. Fuqua, M. I. Savage, C. K. Osborne, S. G. Hilsenbeck, J. C. Chang, G. B. Mills, C. C. Lau, P. H. Brown, *Clin. Cancer Res.* **2015**, *21*, 1688.
[64] J. V. Mccann, J. L. Null, A. C. Dudley, *J.Clinic. Investig.* **2018**, *128*, 2750.
[65] M. Fabre, C. Ferrer, S. Domínguez-Hormaetxe, B. Bockorny, L. Murias, O. Seifert, S. A. Eisler, R. E. Kontermann, K. Pfizenmaier, S. Y. Lee, M. D. M. Vivanco, P. P. López-Casas, S. Perea, M. Abbas, W. Richter, L. Simon, M. Hidalgo, *Clin. Cancer Res.* **2020**, *26*, 3420.
[66] Z. Sun, Y. Hu, C. Wei, R. Hao, C. Hao, W. Liu, H. Liu, M. Huang, S. He, M. Yang, *Carbohydr. Polym.* **2022**, *293*, 119727.
[67] F. Loganzo, M. Sung, H. P. Gerber, *Mol. Cancer Ther.* **2016**, *15*, 2825.
[68] J. Sauveur, L. Conilh, S. Beaumel, K. Chettab, L. P. Jordheim, E. L. Matera, C. Dumontet, *Pharmacol. Res. Perspect.* **2020**, *8*, 11.
[69] F. Loganzo, X. Tan, M. Sung, G. Jin, J. S. Myers, E. Melamud, F. Wang, V. Diesl, M. T. Follettie, S. Musto, M. H. Lam, W. Hu, M. B. Charati, K. Khandke, K. S. K. Kim, M. Cinque, J. Lucas, E. Graziani, A. Maderna, C. J. O'Donnell, K. T. Arndt, H. P. Gerber, *Mol. Cancer Ther.* **2015**, *14*, 952.
[70] A. Marusyk, D. P. Tabassum, M. Janiszewska, A. E. Place, A. Trinh, A. I. Rozhok, S. Pyne, J. L. Guerriero, S. Shu, M. Ekram, A. Ishkin, D. P. Cahill, Y. Nikolsky, T. A. Chan, M. F. Rimawi, S. Hilsenbeck, R. Schiff, K. C. Osborne, A. Letai, K. Polyak, *Cancer Res.* **2016**, *76*, 6495.
[71] D. Ganguly, R. Chandra, J. Karalis, M. Teke, T. Aguilera, R. Maddipati, M. B. Wachsmann, D. Ghersi, G. Siravegna, H. J. Zeh, R. Brekken, D. T. Ting, M. Ligorio, *Cancers (Basel)* **2020**, *12*, 2652.
[72] S. García-Alonso, A. Ocaña, A. Pandiella, *Cancer Res.* **2018**, *78*, 2159.
[73] S. Sousa, R. Brion, M. Lintunen, P. Kronqvist, J. Sandholm, J. Mönkkönen, P. L. Kellokumpu-Lehtinen, S. Lauttia, O. Tynninen, H. Joensuu, D. Heymann, J. A. Määttä, *Breast Cancer Res.* **2015**, *17*, 101.
[74] R. D. Cummings, *Curr. Opin. Struct. Biol.* **2022**, *75*, 102394.
[75] L. Martinez-Pomares, *J. Leukoc. Biol.* **2012**, *92*, 1177.
[76] B. S. Guerrouahen, C. Maccalli, C. Cugno, S. Rutella, E. T. Akporiaye, *Front. Oncol.* **2020**, *9*, 495905.
[77] K. Kawaguchi, M. Sakurai, Y. Yamamoto, E. Suzuki, M. Tsuda, T. R. Kataoka, M. Hirata, M. Nishie, T. Nojiri, M. Kumazoe, K. Saito, M. Toi, *Scientific Rep.* **2019**, *9*, 2924.
[78] B. L. Witt, T. O. Tollefsbol, *Life* **2023**, *13*, 2311.
[79] S. M. Pyonteck, L. Akkari, A. J. Schuhmacher, R. L. Bowman, L. Sevenich, D. F. Quail, O. C. Olson, M. L. Quick, J. T. Huse, V. Teijeiro, M. Setty, C. S. Leslie, Y. Oei, A. Pedraza, J. Zhang, C. W. Brennan, J. C. Sutton, E. C. Holland, D. Daniel, J. A. Joyce, *Nat. Med.* **2013**, *19*, 1264.
[80] L. Xiaocui, H. Wei, C. Yunlang, Z. Zhenzhen, A. Min, *Reprod. Biol. Endocrinol.* **2022**, *20*, 48.
[81] C. H. Ries, M. A. Cannarile, S. Hoves, J. Benz, K. Wartha, V. Runza, F. Rey-Giraud, L. P. Pradel, F. Feuerhake, I. Klaman, T. Jones, U. Jucknischke, S. Scheiblich, K. Kaluza, I. H. Gorr, A. Walz, K. Abiraj, P. A. Cassier, A. Sica, C. Gomez-Roca, K. E. deVisser, A. Italiano, C. LeTourneau, J. P. Delord, H. Levitsky, J. Y. Blay, D. Rüttinger, *Cancer Cell* **2014**, *25*, 846.
[82] H. Jin, V. D'urso, B. Neuteboom, S. D. Mckenna, R. Schweickhardt, A. W. Gross, Y. F. Nanfack, A. Paoletti, C. Carter, L. Toleikis, M. Fluck, J. Scheuenpflug, T. Cai, Y. Fomekong Nanfack, *Oncoimmunology* **2021**, *10*, 1958590.
[83] D. L. Moughon, H. He, S. Schokrpur, Z. K. Jiang, M. Yaqoob, J. David, C. Lin, M. L. Iruela-Arispe, O. Dorigo, L. Wu, *Cancer Res.* **2015**, *75*, 4742.
[84] G. Hu, Y. Su, B. H. Kang, Z. Fan, T. Dong, D. R. Brown, J. Cheah, K. D. Wittrup, J. Chen, *Nat. Commun.* **2021**, *12*, 773.
[85] J. Wen, S. Wang, R. Guo, D. Liu, *Eur. J. Med. Chem.* **2023**, *245*, 114884.
[86] S. P. Rebelo, C. Pinto, N. Lopes, T. R. Martins, P. M. Alves, C. Brito, in *Immuno-Oncology: Methods in Pharmacology and Toxicology*, (Ed.: S. L. Tan), Humana, New York, NY **2020**, https://doi.org/10.1007/978-1-0716-0171-6_8.
[87] F. O. Martinez, S. Gordon, *F1000Prime Rep* **2014**, *6*, 13.
[88] J. Fang, Y. Lu, J. Zheng, X. Jiang, H. Shen, X. Shang, Y. Lu, P. Fu, *Cell Death Dis.* **2023**, *14*, 586.
[89] E. Papalexi, R. Satija, *Nat. Rev. Immunol.* **2018**, *18*, 35.
[90] M. R. Junttila, F. J. de Sauvage, *Nature* **2013**, *501*, 346.
[91] A. F. Labrijn, M. L. Janmaat, J. M. Reichert, P. W. H. I. Parren, *Nat. Rev. Drug Discovery* **2019**, *18*, 585.
[92] S. Li, M. Xia, *Arch. Toxicol.* **2019**, *93*, 3387.
[93] M. E. Boutin, T. C. Voss, S. A. Titus, K. Cruz-Gutierrez, S. Michael, M. Ferrer, *Sci. Rep.* **2018**, *8*, 11135.
[94] D. S. Wishart, Y. D. Feunang, A. C. Guo, E. J. Lo, A. Marcu, J. R. Grant, T. Sajed, D. Johnson, C. Li, Z. Sayeeda, N. Assempour, I. Iynkkaran, Y. Liu, A. MacIejewski, N. Gale, A. Wilson, L. Chin, R. Cummings, D.i. Le, A. Pon, C. Knox, M. Wilson, *Nucleic Acids Res.* **2018**, *46*, D1074.
[95] K. J. Livak, T. D. Schmittgen, *Methods* **2001**, *25*, 402.